# Shearing Melt Out of the Earth: An Experimentalist's Perspective on the Influence of Deformation on Melt Extraction

## David L. Kohlstedt[1] and Benjamin K. Holtzman[2]

[1]Department of Geology & Geophysics, University of Minnesota, Minneapolis, Minnesota 55455; email: dlkohl@umn.edu

[2]Lamont Doherty Earth Observatory, Columbia University, Palisades, New York 10964; email: benh@ldeo.columbia.edu

## Key Words

melt alignment, melt segregation, partial molten rocks, strain localization, anisotropic viscosity

## Abstract

Melt extraction from the Earth's mantle requires some form of channelized flow to produce the observed disequilibrium between the crust-forming lavas and their mantle sources. In this review, we discuss the influence of deformation on melt-extraction processes, with an emphasis on the understanding gained from a wide range of laboratory experimental investigations. Rheological properties of partially molten rocks are very sensitive to melt distribution, and melt distribution is profoundly influenced by deviatoric stress in a viscously deforming partially molten rock, establishing a coupling between deformation and melt distribution. During deformation, this coupling can lead to organization of melt into melt-enriched shear zones at length scales longer than the grain size. We discuss the current state of understanding of this process, with some speculation on its role in the ensemble of processes that constitute melt extraction from the Earth.

## INTRODUCTION

**Melt migration:**
movement of melt down a pressure gradient over distances greater than the grain size

**Melt segregation:**
formation of melt-enriched and melt-depleted regions at length scales longer than the grain size but shorter than the compaction length

**Melt extraction:**
ensemble of processes that lead from formation to emplacement of magmas via segregation and migration by porous flow, fracturing, and melt-rock reactions

Melting in Earth's mantle occurs primarily at plate boundaries and in plumes, which are also regions of intense deformation. Because melt formation and rock deformation coexist in time and space on a large scale, the importance of melt on the viscosity of partially molten rocks has long been appreciated and studied in experiments. Initial laboratory investigations focused on the influence of a melt phase on deformation behavior of partially molten mantle rocks, with emphasis on the dependence of rock viscosity on the amount of melt present as reviewed by Kohlstedt & Zimmerman (1996). More recent experimental studies emphasized the intimately related problem of the effect of viscous deformation on redistributing melt, both by alignment at the grain scale and segregation at larger scales (Kohlstedt & Zimmerman 1996, Zimmerman et al. 1999, Holtzman et al. 2003a,b). This perspective reflected the observation that not only the presence but also the distribution of the melt phase influence large-scale convective flow within our planet (C. Goetze, personal communication). Importantly, the distribution of melt directly affects its rate of transport through the asthenosphere.

Studies of the coupling between melt transport and rock deformation started in the 1970s with analysis of melt migration through the mantle in buoyancy-driven fractures (Weertman 1971) and by porous flow (Ahern & Turcotte 1979, McKenzie 1984). The recognition that chemical disequilibirium between erupted basalt and the rock through which it traveled motivated hypotheses for the development of high-permeability channels (Spiegelman & Kenyon 1992, Hart 1993). Subsequent investigations of the formation of high-permeability, melt-enriched channels followed two distinct but almost certainly coupled routes. First, a series of papers explored channel formation by a reactive infiltration instability mechanism (Daines & Kohlstedt 1994; Aharonov et al. 1995, 1997). As melt ascends adiabatically, it becomes undersaturated in pyroxene. An instability then develops as a result of positive feedback that amplifies local perturbations in melt distribution and thus in permeability (Ortoleva et al. 1987). Second, researchers identified the possibility of channel formation by stress-driven melt segregation (e.g., Stevenson 1989, Kelemen & Dick 1995, Holtzman et al. 2003a,b). In this case, an instability develops as a result of the dependence of rock viscosity on melt fraction. Melt is drawn to local regions slightly enriched in melt as they are weaker and thus at lower mean pressure than those with lower melt content (Stevenson 1989). Again a positive feedback is established that leads to melt segregation and channel growth. Both reactive melt infiltration and stress-driven melt segregation produce melt-enriched, high-permeability channels that isolate the melt phase from the solid residuum, allowing chemical disequilibrium to exist between the ascending magma and the host rock.
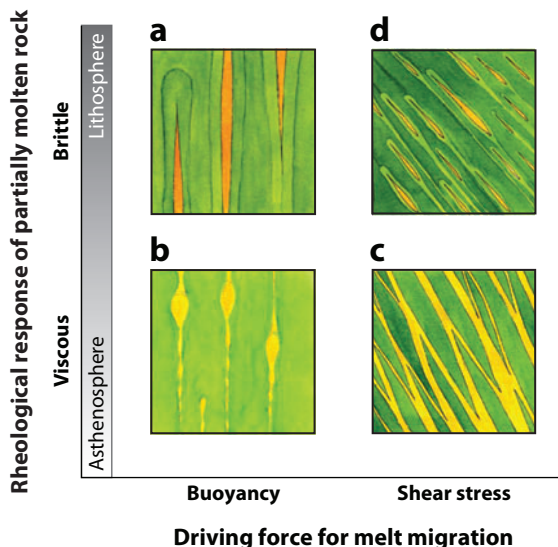
Over the past 20 years, researchers have undertaken theoretical analyses, numerical models, field observations, and laboratory experiments on both analog and natural systems to investigate the dynamics and kinetics of spontaneous melt segregation. In the present paper, we review progress in the area of melt extraction from the mantle, starting with an historical perspective on physical/mechanical mechanisms for channelizing the flow of melt in the asthenosphere. We emphasize in particular experimental investigations of the influence of stress on melt distribution both at the grain scale and at the rock scale, carried out under well-controlled thermo-mechanical conditions with well-defined boundary conditions. Finally, we examine applications of stress-driven melt segregation to Earth both at plate boundaries and in plumes, discussing the process of extrapolating the results of laboratory experiments to the longer temporal and spatial scales of geological processes.

## HISTORICAL BACKGROUND

Our understanding of the mechanisms and kinetics of melt extraction from Earth's mantle has evolved as constraints from field observations, theoretical analyses, and experimental

measurements provide new insights into the physical paths, spatial extent, and temporal duration of melt transport. Evidence for melt movement both by porous flow through hot, viscously deforming partially molten rocks at depth and by injection of magma into fractures in cooler, more brittle rocks in the shallower lithosphere are observable in ophiolites (Nicolas 1989, Kelemen et al. 1997) and orogenic lherzolites (Le Roux et al. 2008, Kaczmarek & Müntener 2008). The mantle sections exposed in ophiolites reveal evidence for both brittle and viscous processes of magma transport. To address the question of which processes dominate melt transport in the mantle, the effects of physical and chemical conditions on the behavior of partially molten rocks must be investigated with observations from experiments and nature.

As illustrated in the melt-migration mechanism map in **Figure 1**, a range of driving forces and of response mechanisms define thermo-mechanical regimes for melt transport through the mantle. The driving forces for movement of melt include buoyancy forces due to the differences in density between the melt and the residual rock and pressure gradients caused by shear deformation of a partially molten rock. Possible response mechanisms involve magma injection into dikes that form by brittle deformation and porous flow of melt through melt-enriched channels that develop during viscous deformation of partially molten rock. Here we discuss each quadrant in **Figure 1** in an historical context; in addition, we introduce the role of melt-rock reaction in magma transport.

**Ophiolite:** fragment of oceanic crust and uppermost mantle usually formed at a spreading center and subsequently obducted onto the continental crust



**Figure 1**

Melt-migration mechanism map. Mechanisms of melt migration through partially molten mantle rocks are defined in terms of the driving force causing melt migration and/or melt segregation and by the deformation response of the rock. Driving force ranges from buoyancy to shear stress, while deformation response ranges from brittle to viscous. The vertical axis corresponds to the Deborah number, $De$, which is the ratio of the viscoelastic relaxation time of the matrix to the characteristic timescale of observation of the melt migration process. If the characteristic time is less than the relaxation time, then the effective matrix rheology response to the strains associated with melt migration will be elastic. The horizontal axis compares the gravitational energy released by ascending melt to the strain energy released by the matrix during melt migration. The melt-migration mechanism cartoons in this figure represent (*a*) tensile dike propagation in the brittle regime, (*b*) porous flow and porosity waves in the viscous regime, (*c*) stress-driven melt segregation in the viscous regime, and (*d*) shear crack propagation in the brittle regime. The gradient bar to the right of the y axis indicates the separation of brittle processes expected to dominate in the lithosphere from viscous mechanisms anticipated to govern in the asthenosphere. Modified from Phipps Morgan & Holtzman (2005).

## Buoyancy-Driven Melt Transport Through Brittle Fractures

**Pore versus void:**
melt-filled plus vacant space versus vacant space

Perhaps because magma intrusion through dikes forms much more obvious features than those produced by melt transport by porous flow, the postplate tectonic inquiry into the melt extraction problem began with the question of how deep dikes could exist in the mantle. This regime forms the upper left quadrant of the melt-migration mechanism map in **Figure 1** in which melt flow is driven by a buoyancy force and the rock responds by brittle fracture. Weertman (1971) developed an analogy between water transport through hydro-fractures in glaciers and magma transport through dikes in the mantle. Nicolas (1986) championed the idea that most of the melt flux in the asthenosphere occurs through dikes, based on observations of gabbro dikes in the mantle section of the Oman ophiolite. Theoretical studies on the viability of fracture at high temperature and high confining pressure demonstrate that a magma-filled dike must attain a minimum volume in order to generate enough buoyancy force to fracture the overlying rock and propagate upward (e.g., Spence & Turcotte 1985, Spence et al. 1987, Sleep 1988). This requirement poses a significant limitation. Since the fracture strength of a rock mass is more easily overcome at lower temperatures at which creep cannot relax tensile stresses at the tips of the crack, dikes are more likely to form in the conductively cooling regions of the lithospheric mantle than in the hotter asthenosphere. More recently, other researchers have explored the influence of a viscoelastic, porous matrix on propagation of hydro-fractures or magma-fractures (e.g., Fowler & Scott 1996; Rubin 1993, 1998), moving toward the middle ground between brittle and viscous end-member processes.

## Buoyancy-Driven Melt Migration by Porous Flow

At the higher temperatures characteristic of the asthenospheric mantle, melt migrates by porous flow through a viscous matrix. This regime is depicted in the lower left quadrant of **Figure 1** in which melt flow is driven by a buoyancy force and the partially molten rock responds by viscous flow. In this regime, the high stresses required for dike formation cannot build up owing to their relaxation by high-temperature creep processes. In the mantle at high confining pressure, void (empty) space cannot open, thus any change in melt fraction due to melt migration must, in the absence of melting and/or crystallization, be balanced by flow of the solid matrix (pore versus void). This constraint couples the melt flux to the solid flux. The two-phase viscous flow equations describing these coupled fluxes are referred to as magma dynamics or compaction theory. Initially developed by Drew (1983), the theory was applied to Earth by several authors (e.g., McKenzie 1984, Scott & Stevenson 1984, Fowler 1985, Ribe 1986). Their analyses then took two general directions. First, one solution of these equations led to development of solitary waves (e.g., Scott & Stevenson 1984, Spiegelman 1993). Although these waves are difficult to observe in Earth, they do form in tank experiments on analog systems (e.g., Scott et al. 1986, Whitehead 1987). More recently, a study on the importance of viscoelasticity in the compaction process produced a localization phenomenon that begins to resemble a dike (Connolly & Podladchikov 1998, 2007).

The second approach focused on the chemical interactions between the melt and the residual rock, keeping the migration dynamics relatively simple (e.g., McKenzie 1984, Richter & McKenzie 1984). Several types of observations require that most of the melt extracted to produce oceanic crust is not in chemical equilibrium with the mantle through which it passed (e.g., Kelemen et al. 1997). Hence melt must be removed relatively quickly from the mantle such that the degree of chemical equilibrium with mantle rocks during upward migration is small. This observation indicates that much of the melt transport must occur in chemically isolated, high-permeability channels (e.g., Spiegelman & Kenyon 1992). Trace element disequilibrium between mid-ocean

ridge basalts (MORBs) and abyssal and ophiolitic peridotites (e.g., Johnson et al. 1990) supports this conclusion. Subsequently, MORB was found to be in equilibrium with dunite bodies but not with the surrounding peridotite, as observed in the Oman and other ophiolites, indicating that dunites are chemically isolated pathways through which melt is transported to near Earth's surface from deep within the upper mantle (e.g., Kelemen et al. 1995). The requirement for chemical disequilibrium has significantly influenced the development of ideas on the thermal-chemical-mechanical models for melt extraction.

## Stress-Driven Melt Migration in the Brittle Regime

Phipps Morgan & Holtzman (2005) proposed a process for melt transport by which shear stress can drive the migration of melt-filled cracks (referred to as vug waves) parallel to the shear plane, analogous to the motion of dislocations in a deforming crystal or propagation of mode-II cracks. This regime is illustrated in the upper right quadrant of the melt-migration mechanism map in **Figure 1** defined by melt migration in response to a shear stress under conditions for which the rock responds by deforming in a brittle manner. These moving shear cracks are driven by the release of elastic shear strain energy and restrained by the viscous dissipation in the fluid. Although melt-filled cracks aligned in the shear plane are observed in shear zones in exposures of deep crust (see references in Phipps Morgan & Holtzman 2005), the process has yet to be fully explored in theoretical analyses or directly observed in experimental studies.

## Stress-Driven Melt Segregation in the Viscous Regime

Stevenson (1989) proposed a simple but elegant model for a process by which melt would spontaneously segregate into melt-enriched channels driven by perturbations in differential stress in a deforming viscous, two-phase system. This regime forms the lower right quadrant of the melt-migration mechanism map in **Figure 1**. In this model, the instability proceeds because the composite viscosity is very sensitive to the melt fraction, so that small perturbations in melt fraction cause associated spatial variations in viscosity and thus in shear stress. The perturbations in shear stress translate into gradients in mean pressure that drive melt from regions with lower melt fractions to areas with higher melt fractions. Thus a positive feedback system is set up such that the perturbations grow with continued deformation until melt is nearly completely extracted from the regions between melt-enriched layers. This idea was explored further in theoretical papers by Richardson et al. (1996) and Hall & Parmentier (2000), among others. In our experimental studies of shear deformation of partially molten rocks (e.g., Holtzman et al. 2003a, Holtzman & Kohlstedt 2007), we demonstrated that melt does indeed segregate and self-organize into melt-enriched bands driven by stress during deformation in the viscous regime. This review focuses on melt transport in this viscous regime, emphasizing stress-driven alignment of melt at the grain scale and spontaneous segregation and organization of melt at a larger scale in deforming partially molten rocks.

## Reaction-Driven Melt Segregation

**Figure 1** could be extended into a third dimension in which reactions between the melt and the solid rock are taken into account. The recognition of the role of dunite bodies as melt extraction pathways led to the development of models of channel formation by dissolution reactions. Based on a model of Chadam et al. (1986), a reaction infiltration instability (RII) occurs in mantle rocks because the dissolution of clinopyroxene out of the peridotite host into the basaltic melt leads to
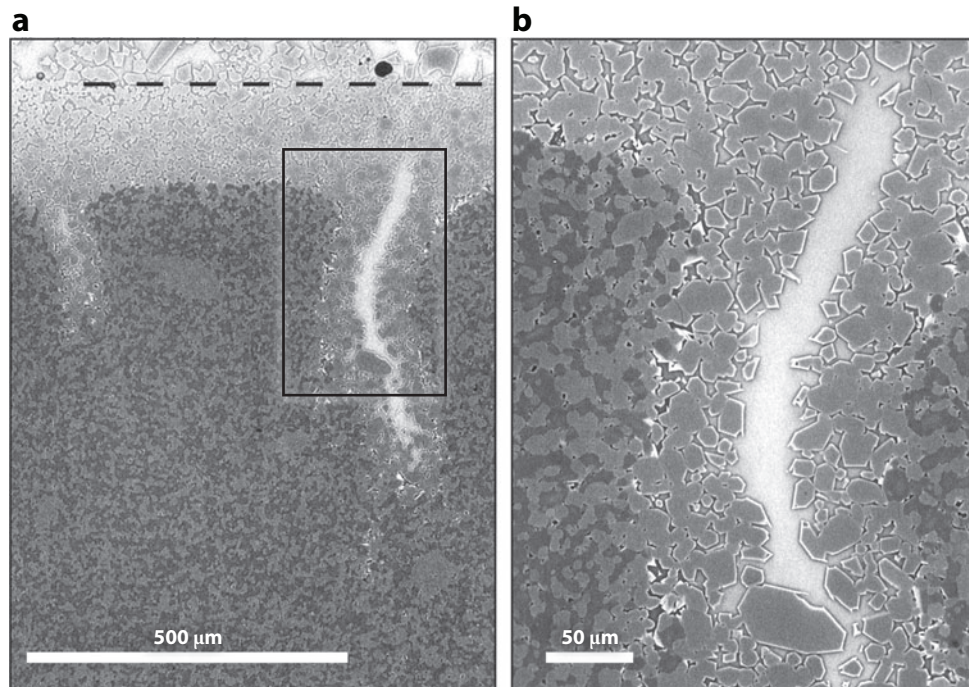
**Figure 2**

Backscattered-electron micrographs of reaction infiltration instabilities in a melt migration couple formed between a disc of olivine + 50% clinopyroxene (*bottom*) and a disc of melt undersaturated in clinopyroxene (*top*). The initial interface between the two discs is marked by the horizontal dashed line in (*a*). The reaction front instability extends into the olivine + clinopyroxene disc as finger-like protrusions, two of which are captured in this image. The center of the larger instability on the right is composed entirely of glass, that is, quenched melt (*white*). The melt is separated from unreacted matrix of olivine (*light gray*) + clinopyroxene (*dark gray*) by a layer of olivine that formed by precipitation from the melt as the melt dissolved clinoproxene from the two-phase disc. The enlargement of the region outlined by the box in (*a*) provides a more detailed view of the reaction infiltration instability in (*b*).

increased porosity and permeability. Further melt transport is thus enhanced by the dissolution reaction because, as the melt migrates upward to lower pressure, the solubility of clinopyroxene in the melt increases, producing a solubility gradient (Kelemen et al. 1995). This process results in a channel-forming instability in which the channels have a dunite composition, as demonstrated in the laboratory experiments of Daines & Kohlstedt (1994) and illustrated in **Figure 2** (see also, Aharonov et al. 1995, Kelemen et al. 1995, Morgan & Liang 2005). Thus, the debate concerning the mechanism of melt extraction from the mantle was cast in terms of dunite channels versus dikes or, in the terms used in this review, viscous versus brittle control on the dominant mechanism of melt transport.

## Summary of Melt-Migration Mechanisms

Our purpose here is not to assess the successes and failures of each of the mechanisms described above in explaining all of the observations and constraints. It is clear that dikes and dunite channels exist in ophiolites and peridotite massifs and that they transported melt. Melt migration is complex in part because the rheological control on the process is sensitive to time and length scales and

because, as melt migrates from its source to the surface, it passes through a range of conditions in which the thermodynamic state and thus material properties change. All of the processes described in the preceding paragraphs may be important at some location along the path traversed by melt moving from its source to the surface. While melt-migration mechanisms control the kinetics and extent of melt-rock interaction, these properties are also directly influenced by melt-rock reactions. In the following sections, we focus on the mechanical processes, but the reader should bear in mind the possible influence of melt-rock reactions on mechanical properties as well as on melt transport.

## STRESS-DRIVEN MELT REDISTRIBUTION IN PARTIALLY MOLTEN ROCKS UNDERGOING DEFORMATION

In the absence of deviatoric stress (i.e., under a hydrostatic state of stress), the distribution of melt in a partially molten rock is controlled by interfacial tension. The resulting melt topology is generally characterized by the dihedral angle, $\theta$, which is determined by the relative values of the solid-melt and solid-solid interfacial energies, $\Gamma_{sm}$ and $\Gamma_{ss}$, through the expression $\cos(\theta/2) = \Gamma_{ss}/2\Gamma_{sm}$. For the partially molten, upper mantle rocks of interest in this review, the dihedral angle lies in the range $10° < \theta < 50°$ (e.g., Kohlstedt 1992, Holness 2006) such that the melt forms an interconnected network along three- and four-grain junctions (i.e., grain edges and corners) at least for minerals with single-valued interfacial energies (Waff & Bulau 1979, 1982; von Bargen & Waff 1986). However, melt often extends into some grain-grain interfaces (i.e., grain boundaries and phase boundaries) due to anisotropy in $\Gamma_{sm}$ and $\Gamma_{ss}$, that is, these interfacial energies are not single-valued quantities (Cooper & Kohlstedt 1982, Waff & Faul 1992, Faul et al. 1994). The fraction of grain and phase boundaries wetted, in this case, increases with increasing melt fraction, φ (Hirth & Kohlstedt 1995a,b; Yoshino et al. 2005).

In the presence of a nonhydrostatic state of stress, melt topology and distribution differ significantly from the case in which they are controlled by interfacial tension alone. In the following sections, we review the effects of stress on the distribution and organization of melt during deformation of partially molten rocks. We distinguish among several categories of stress-driven behavior including (*a*) redistribution of melt at the grain scale (alignment), (*b*) movement of melt over distances greater than the grain scale in response to externally imposed pressure gradients (imposed migration), and (*c*) organization of melt over distances greater than the grain scale in response to pressure gradients that develop spontaneously in a partially molten rock during deformation (spontaneous segregation).

The response of the melt topology and distribution to an applied stress in the viscous regime depends on the experimentally imposed boundary conditions and the rheological properties of the partially molten system. The mechanical properties of a partially molten rock can be represented in terms of the compaction length, $\delta_c$, a critical scale length arising from two-phase flow theory (e.g., McKenzie 1984). The compaction length is determined by the flow properties of the fluid and the solid as

$$\delta_c = \sqrt{\left(\frac{k}{\mu}\right)\left(\eta + \frac{4}{3}\zeta\right)}, \tag{1}$$

where $k$ is the permeability of the solid to flow of melt, $\mu$ is the viscosity of the melt, and $\eta$ and $\zeta$ are the shear viscosity and bulk viscosities of the partially molten rock, respectively. Physically, the compaction length describes the length scale over which gradients in melt pressure and melt fraction can be sustained within a deforming two-phase system; over this distance, the flow of the solid and flow of the melt are coupled. Conceptually, this length scale is fundamental to

understanding the variety of responses to experimentally imposed boundary conditions discussed below. A number of the experimental geometries utilized to investigate deformation of partially molten natural and analog materials are summarized in **Figure 3** and discussed in more detail below.
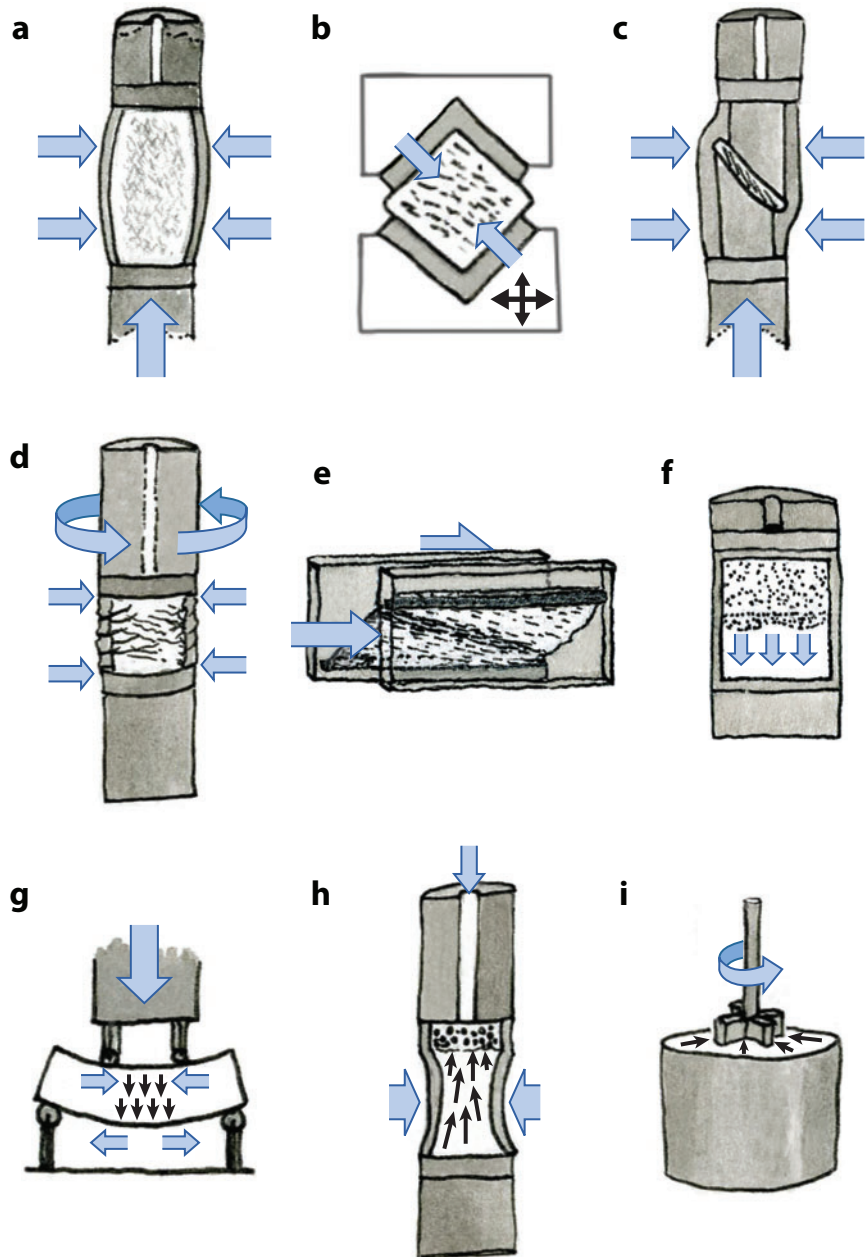
## Stress-Driven Alignment of Melt During Shear Deformation

In response to a deviatoric stress, melt locally (i.e., at the grain scale) rearranges and assumes a pronounced melt-preferred orientation (MPO). In triaxial compression experiments (**Figure 3***a*), melt does not align parallel to the maximum principle stress, $\sigma_1$, (Bussod & Christie 1991, Beeman & Kohlstedt 1993, Jin et al. 1994, Kohlstedt & Zimmerman 1996, Bai et al. 1997, Daines & Kohlstedt 1997, Zimmerman & Kohlstedt 2004). Instead the melt-preferred orientation occurs at angles of 15° to 30° to $\sigma_1$ (Daines & Kohlstedt 1997). No evidence was observed for micro-cracking. Similar conclusions concerning stress-induced alignment of melt pockets in partially molten samples of borneol + melt, viscously deformed in uniform pure shear tests (**Figure 3***b*), were reached based on analyses of in situ monitoring of splitting of ultrasonic shear waves (Takei 2001). Consistent with an interpretation of a viscous mechanism for alignment of melt pockets, a finite amount of time was required for melt to redistribute in response to a change in applied stress.

In partially molten rocks deformed in geometries that produce a significant component of simple shear, such as direct shear (**Figure 3***c*), torsion (**Figure 3***d*), and see-through simple shear tests (**Figure 3***e*), a marked alignment of melt pockets also occurs. The examples of the melt distribution in an undeformed and a deformed aggregate of partially molten olivine plus basalt in **Figure 4** demonstrate the dramatic realignment of melt that occurs in response to a nonhydrostatic state of stress (Zimmerman & Kohlstedt 1996, Zimmerman et al. 1999). While the melt distribution is isotropic in the undeformed sample, a clear melt-preferred orientation developed in the sample deformed in direct shear. The melt pockets are elongated and aligned at an angle of ~20° to the shear plane in a direction antithetic to the shear direction. As discussed below in reference to **Figure 5** in the section on Theoretical Considerations, locally high tensile stresses at solid-melt-solid triple junctions can be relaxed by wetting grain boundaries to produce this MPO (Hier-Majumder et al. 2004). See-through shear tests (**Figure 3***e*) on samples of norcamphor plus molten benzamide under drained conditions also result in a melt-preferred orientation subparallel to the shortening direction; however, in this case, the authors argue that their melt distribution results from dynamic wetting of grain boundaries due to intergranular microfracturing (Rosenberg & Handy 2000).

## Imposed Migration of Melt in a Pressure Gradient

At least four different types of experimental tests have been used to explore the migration of melt in response to externally imposed pressure gradients. In these experiments, pressure gradients

←———————————————————————————————————————————

**Figure 3**

Sketches illustrating the various types of experiments that have been used to study melt migration and melt segregation in partially molten rocks. (*a*) Triaxial compression produces pure shear except near the top and bottom of the sample due to friction between the sample and the pistons, the triaxial compression test. (*b*) Deformation apparatus yields pure shear uniformly through a sample, the uniform pure shear test. (*c*) Direct shear results in transpressional deformation with a large component of simple shear and smaller component of compressive strain, the direct shear test. (*d*) High-pressure torsional deformation provides simple shear, the torsion test. (*e*) Displacement of the upper glass slide over the lower glass slide produces simple shear under drained conditions, the see-through shear test. (*f*) Melt-migration couple draws melt from the high melt fraction disc at the top into the low melt fraction disc at the bottom, the sponge test. (*g*) Four-point bending of a partially molten sample drives melt from the high-pressure compressive region to the low-pressure tensile region, the flex test. (*h*) Reducing the pore pressure below the confining pressure forces melt out of a partially molten sample, the toothpaste tube squeeze test. (*i*) Rotation of a vane immersed in a partially molten sample causes migration of melt from the outside toward the inside, the paddle wheel test.
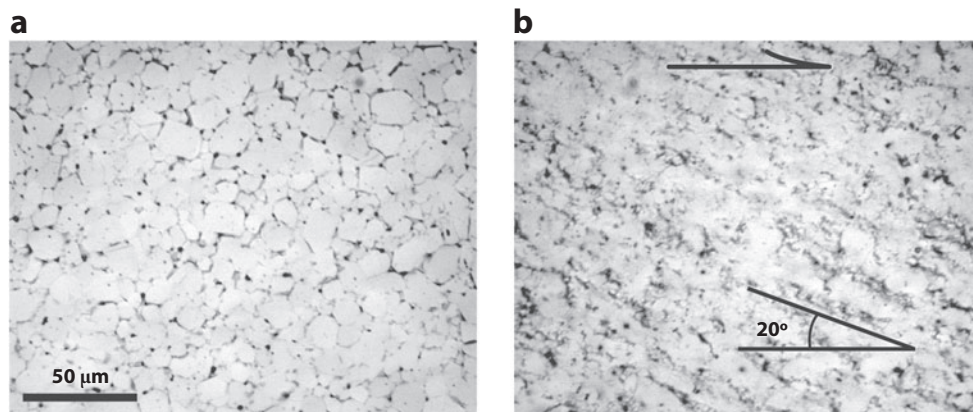
**Figure 4**

Reflected light optical micrographs of (*a*) an undeformed sample and (*b*) a sheared sample of olivine plus
3 vol% MORB. In the undeformed sample in (*a*), melt (*darker gray*) is randomly distributed in three- and
four-grain junctions separating olivine grains (*lighter gray*); some grain boundaries are also wetted by the
melt. A few, usually spherical voids (*black*) are present, primarily in the melt but occasionally in the olivine. In
the deformed sample in (*b*), melt is well aligned at ∼20° to the shear plane, which is horizontal in this figure,
producing a pronounced melt-preferred orientation. Melt segregation does not occur at a length scale
greater than the grain size. Modified from Xu et al. (2004) and Kohlstedt (2007).
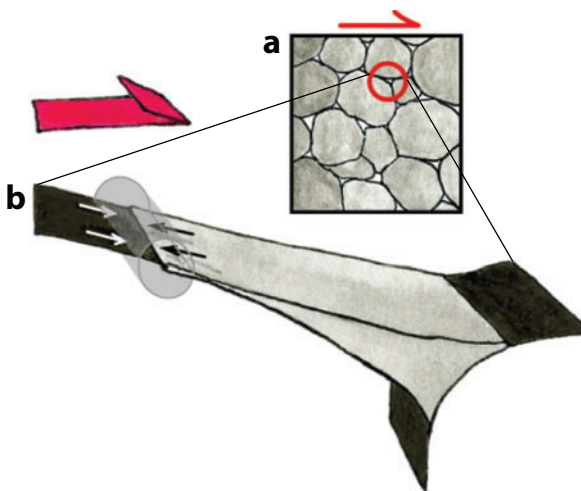


**Figure 5**

Sketch illustrating the effect of shear stress on establishing a melt-preferred orientation based on the model
of Hier-Majumder et al. (2004). (*a*) View of a section through a partially molten rock with θ < 60° such that
melt is present in all of the triple junctions, indicative of a melt that forms an interconnected grain-scale
network in three dimensions. (*b*) Enlarged view of the triple junction that is circled in (*a*). Due to the applied
far-field shear stress, a localized tensile stress arises at the tip of this appropriately oriented triple junction.
Melt extends into the grain boundary to relax the stress, resulting in partial or complete wetting of the grain
boundary.

were established by controlling either the initial melt distribution or the applied state of stress. The experimental geometries are summarized in **Figure 3f–i**.

A gradient in melt fraction within an otherwise homogeneous partially molten rock sets up a gradient in effective pressure in the melt phase (Stevenson 1986). As a result, melt migrates from regions of higher melt fraction to regions of lower melt fraction (sponge test, **Figure 3f** ). Two experimental approaches have been taken to study this phenomenon. First, in a melt-migration couple composed of a source and a sink, melt is drawn from the region with the higher melt fraction into the region with lower melt fraction (Watson 1982; Riley et al. 1990; Riley & Kohlstedt 1990, 1991; Daines & Kohlstedt 1993). Second, homogenization of a heterogeneous melt distribution during static annealing of samples containing melt-enriched bands, previously generated by shear deformation (e.g., Holtzman et al. 2003a,b), is driven by the gradient in interfacial energy (surface tension) and pressure that are associated with the gradient in melt fraction (Parsons et al. 2008). Although interfacial energy provides a relatively small driving force at the large length scales appropriate to Earth, it dominates over buoyancy forces at the scale of a laboratory experiment. Nonetheless, analysis of melt redistribution in response to a gradient in melt fraction (gradient in surface tension) provides one method of exploring aspects of compaction theory.

In a series of four-point bending experiments (flex test, **Figure 3g**) on samples composed of fine-grained orthoenstatite with 5 vol% of an aluminosilicate glass, the volume fraction of melt on the tensile side of the deformed sample exceeded that on the compression side by a factor of greater than three (Cooper 1990). In this example, melt migrated in response to the gradient in mean pressure established by the gradient in applied stress. The results were successfully modeled in terms of a combination of anelastic (time-dependent but recoverable) deformation and steady-state creep (time-dependent and non-recoverable deformation). The resulting melt profile reflected a balance between melt being driven from the compression side to the tension side by the gradient in applied stress and melt being driven from the tension side back to the compression side by the gradient in melt fraction. These experiments illustrate elements of compaction theory for two-phase flow with the compression side compacting by deformation of the solid matrix combined with flow of melt toward the tensile side and, in turn, the tension side decompacting by deformation of the solid matrix coupled with flow of melt from the compression side. The rates of compaction and decompaction were controlled by the rate of deformation of the solid phase, that is, by the viscosity of the solid phase as expressed in Equation 1.

With a pressure gradient imposed through a difference between confining pressure and pore fluid pressure (toothpaste tube squeeze test, **Figure 3h**), melt extraction from partially molten samples of olivine plus several percent of a silicate melt into a porous reservoir provided a measure of permeability and bulk viscosity and thus of compaction length (Renner et al. 2003). Compaction length was varied in these experiments by using melts of very different compositions and thus significantly different viscosities. No gradient in melt fraction developed in samples containing a low-viscosity melt. However, a marked gradient in melt fraction formed in samples containing a high-viscosity melt. In the former case, compaction rate is limited by compaction of the solid grains as melt migration is relatively easy for the low-viscosity melt; furthermore, the compaction length is large compared to the sample length. In the latter case, compaction rate is governed by flow of the more viscous melt, a case for which the compaction length is smaller than the sample size.

In rotary shear experiments carried out in a four-vane apparatus on hypoeutectic metal alloys (paddle wheel test, **Figure 3i** ), deformation is applied while the molten material crystallizes, forming a solid-supported matrix of dendrites (Gourlay & Dahle 2007). While deforming in the solid-supported state, melt segregates toward the rotating vanes. In this geometry, a stress gradient exists within the solid. The melt is migrating down a gradient in fluid pressure that results from dilation of the sample close to the spinning paddle wheel where stresses in the solid framework

are highest. Although conditions are far from those in the deep Earth, this migration of fluid up a gradient in stress in the solid has intriguing implications for melt segregation and lubrication of boundary layers in partially molten regions (Takei & Holtzman 2009c).

## Spontaneous Segregation and Organization of Melt During Shear Deformation

**Behavior across the brittle-viscous spectrum.** Spontaneous self-organization of melt that occurs inside a deforming sample without the imposition of a pressure gradient across the sample is distinct from the behaviors discussed above. Segregation and organization are produced during deformation by the development of local pressure gradients over length scales longer than the grain size but shorter than the sample thickness. In flow dominated by simple shear, melt segregates into melt-enriched bands or layers that also concentrate strain, forming networks of shear zones. This type of behavior occurs in a very wide range of materials, from sands and clays deforming in the brittle-granular regime to partially molten rocks deforming in the viscous regime. Here we first discuss this range of systems and then focus on experiments on partially molten systems at high temperature. Subsequently we review models describing the mechanisms for the formation of such organized structures.

On the brittle end of the brittle-viscous spectrum in **Figure 1**, deformation experiments are performed on brittle/granular fault gouge materials to understand their frictional properties; in this regime, deformation is dilatant and thus strength is pressure-sensitive (for a review see Marone 1998). During deformation, arrival at the yield strength of the material is associated with the onset of localization on bands oriented at ∼20° to the shear plane and antithetic to the shear direction, followed by weakening and the onset of steady sliding. These shear bands are classified as Riedel or $R_1$ shears. Riedel shears are associated with a specific ratio of local dilatancy and shear displacement, as well as shear stress and normal stress (i.e., the friction coefficient). The dilatancy mechanism is granular flow in which void space opens as rigid grains slide past one another. The steady sliding is associated with deformation on bands that are parallel to the shear plane and therefore nondilatant (Rudnicki & Rice 1975, Bésuelle 2001).

In the transitional region of the brittle-viscous spectrum (often referred to as semibrittle or brittle-ductile), localization of deformation and redistribution of fluid/gas phases are associated spatially and temporally with each other, accommodated by both crystalline creep and brittle fracture processes. A study of deformation of a quartz-water system revealed the formation of continuous (Riedel) bands enriched in water-filled pores during semibrittle deformation/granular flow (Schmocker et al. 2003). Torsion experiments (**Figure 3d**) were carried out to high shear strains at high pressures and temperatures under drained conditions. The authors observed a hardening behavior that they associate with fluid segregation. This hardening is associated with the formation of interconnected pores along planes oriented at 20° and 70° to the shear plane, antithetic to the shear direction. This interconnected pore structure evolved into bands as fluid flowed into and drained along them during deformation. A similar semibrittle localization behavior was observed in a study of fine-grained feldspar aggregates containing <3 vol% of a silica-rich glass and a gas phase (Rybacki et al. 2008). During deformation, both the melt phase and the gas phase segregated into bands, producing cavitation within the melt-enriched bands. These experiments were again performed in torsion to large strains at high pressures and temperatures but under undrained conditions. The bands developed at an angle of 15°–30° to the shear plane, antithetic to the shear direction. Some samples failed abruptly as cavities nucleated, grew, and coalesced. While the anorthite grains deformed by viscous (diffusion and dislocation) mechanisms (more so than the quartz in the study of Schmocker et al. 2003), the locally high concentrations of the gas phase facilitated cavitation and fracture.

**Ductile:** ability of a material to deform plastically/viscously without fracture

Such semibrittle behavior is also observed in crystalline organic materials used as analogs for partially molten earth materials. Simple shear experiments on partially molten aggregates of nor-camphor + benzamide under drained conditions in a see-through glass slide apparatus (**Figure 3e**) produced melt-bearing, extensional shear fractures (Rosenberg & Handy 2000). Interconnection of these features resulted in melt-enriched shear bands. Melt was rapidly expelled from the shear bands into the low-pressure regions in adjacent, nondeforming portions of the sample. In pure shear experiments with a see-through glass slide apparatus on undrained samples of norcamphor + ethanol and of $KNO_3$-$LiNO_3$, deformation occurred by a variety of mechanisms including grain boundary sliding, grain boundary rupturing, dislocation creep, and granular flow (Walte et al. 2005). In samples with a melt fraction of ~0.08, deformation by grain boundary sliding becomes localized in melt-enriched conjugate shear zones.

The influence of stress on melt distribution in organic materials can also be studied in the viscous regime (**Figure 1**). In uniform pure shear experiments on samples of borneol + melt, melt-enriched sheets formed roughly in shear planes (Takei 2005). In samples with initially homogeneous melt distributions, a single melt sheet formed. Microscopically the melt sheet was composed of wetted grain boundaries with a thickness of about one grain. In samples with initially heterogeneous melt distributions, several melt sheets formed parallel to the conjugate shear planes. Note that initial heterogeneities in melt distribution (e.g., large melt pools) were decreased due to deformation, requiring large-scale melt flow. The author suggested that the melt-enriched sheets may have formed by infiltration of melt coupled with dissolution of solid material at stress concentrations that occur at solid-solid-melt junctions; this dissolved material then precipitates at unstressed regions of the sample.

The influence of stress on melt distribution in partially molten upper mantle rocks can also be investigated in the viscous deformation regime (**Figure 1c**). In direct shear experiments (**Figure 3c**) on samples of olivine + MORB, grain-scale melt alignment occurred at ~20° to the shear plane, antithetic to the shear direction, as discussed above. In similar experiments on a wide range of partially molten rocks with compaction lengths shorter than that for samples of olivine + MORB, stress-driven melt segregation resulted in the formation of melt-enriched bands oriented ~20° to the shear plane, antithetic to the shear direction (Holtzman et al. 2003a). Sample compositions included olivine + MORB + solid chromite, olivine + MORB + molten iron sulfide, olivine + albitic melt, and anorthite + basalt. These compositions represent ranges in solid and melt viscosity as well as a range in permeability. Although the morphologies (e.g., thickness of and spacing between melt-enriched bands) differed among samples, the general character of the microstructure was similar from one sample to the next.

The brittle-viscous spectrum discussed above can be summarized by introducing the Deborah number, $De$, which is defined as the ratio of the relaxation time, $t_r$, that characterizes the intrinsic fluidity of a material, to the process time scale, $t_p$, that characterizes an experiment or a computer simulation probing the response of the material (**http://en.wikipedia.org/wiki/Deborah_number**):

$$De = \frac{t_r}{t_p}. \tag{2a}$$

The relaxation time can be expressed as $t_r \approx \eta/E$ and the process time scale can be approximated as $t_p \approx 1/\dot{\varepsilon}$ such that

$$De \approx \frac{\eta \dot{\varepsilon}}{E}. \tag{2b}$$

Smaller values of $De$ favor viscous behavior, whereas larger values of $De$ encourage brittle response. Therefore, viscous rather than brittle deformation occurs if viscosity is small (i.e., temperature is
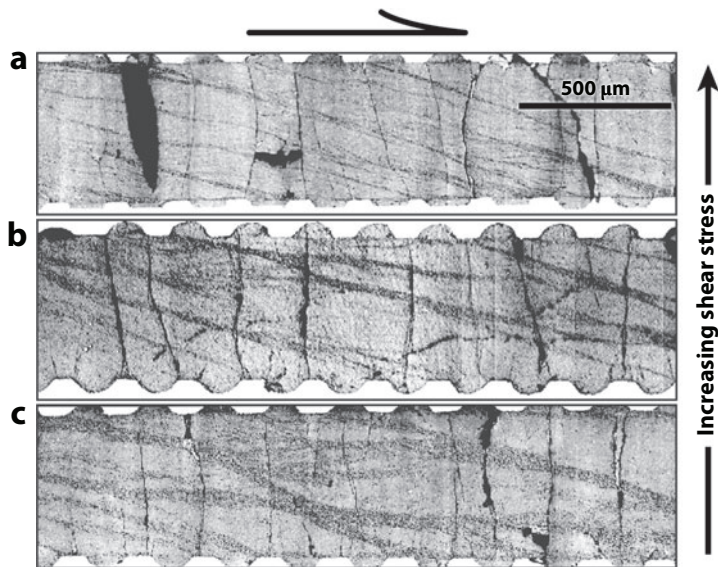
high) and/or strain rate is slow. In a partially molten system, both viscosity and elastic modulus decrease with increasing melt fraction (Takei 1998).

Across a wide range of mechanical response from brittle to viscous, segregation features form at ~20° to the shear plane, antithetic to the shear direction. The local change in porosity by granular dilatancy is related to the local ratio of shear stress to normal stress (Rudnicki & Rice 1975, Bésuelle 2001). Viscous decompaction may have the same ratio of shear stress to normal stress; however, the accommodation mechanism for the local volume change differs along the spectrum from brittle/granular to ductile. For dilatation of a partially molten system, the volume of the sample increases as empty (as opposed to melt/fluid filled) porosity and/or cracks open in regions in which strain is localizing. Melt will flow into these low-pressure regions. In confined high-temperature magmatic systems, empty space is not created; changes in melt fraction are accommodated locally by melt migration coupled with matrix deformation, that is, by compaction and decompaction in regions in which melt fraction is decreasing and increasing, respectively. Viscous deformation mechanisms involving diffusion, dislocation, grain boundary sliding, and/or solution-precipitation processes relax stress concentrations that develop within a deforming rock thus inhibiting cavitation, fracture, and granular flow.

In the following discussion, we focus on experiments in which the materials are deforming in the ductile (viscous) regime and are nondilatational. We demonstrate an internally consistent scaling of both the occurrence of the segregation process and the spacing of the melt-enriched networks using the compaction length. These constraints suggest the appropriateness of application of viscous two-phase flow theory to these systems.

**Behavior in the viscous regime.** To further investigate stress-driven melt segregation and organization, we explored the effects of stress and strain on the details of the morphology of melt-enriched bands in the system olivine + chromite + MORB (Holtzman & Kohlstedt 2007). Melt bands are clearly visible by a shear strain of $\gamma \approx 1$. In three samples, each deformed at a different stress level in direct shear to $\gamma > 3$ (shown in **Figure 6**); the spacing between the largest melt-enriched bands in the network is inversely proportional to the stress level. Our measurements also demonstrate that, in a given sample, the density of thin bands is larger than the density of thick bands and thinner bands lie at lower angle to the shear plane than thicker bands. The resulting anastomosing network of connected bands decreases the viscosity and increases the permeability in the sample, both as anisotropic properties that are enhanced parallel to the bands. The increase in permeability was estimated in Holtzman et al. (2003a).

A major limitation in direct shear experiments (**Figure 3c**) is the small sample size (<1 mm thick), a difficulty that is overcome to a significant degree in torsion experiments (**Figure 3d**) in which samples are significantly larger (>5 mm thick). Furthermore, in the torsion geometry, the strain and strain rate are zero along the rotation axis of the sample and increase to maxima at the outer radius, while stress increases linearly or nonlinearly depending on the deformation mechanisms in the material (Paterson & Olgaard 2000). Thus, a large range of stress, strain, and strain rate conditions can be studied in a single experiment, in effect sampling an evolution of the system. Comparison of the microstructures of samples of olivine + chromite + 4% MORB in **Figures 6** and **7** demonstrates that the melt-enriched bands have significantly more room to organize in samples deformed in torsion than in those deformed in the direct shear (King et al. 2007). The bands extend from the edge toward the center of the sample to a radius that corresponds to $\gamma \approx 1$. The band spacing is similar to that observed in samples deformed in direct shear, indicating that the spacing does not depend on the sample size but is controlled by the physical properties of the system as encapsulated in the compaction length.

**Dilatation:** in this review, volume increase of melt-rock system due to growth of voids and cracks

**Increasing shear stress**

**Figure 6**

Reflected light optical micrographs of melt-enriched bands that formed at ∼20° to the shear plane in three samples of 72% olivine + 24% chromite + 4 vol% MORB deformed in direct shear to $\gamma \approx 3.5$ at shear stresses of (*a*) 58 MPa, (*b*) 116 MPa, and (*c*) 177 MPa. The melt-enriched bands are darker gray than the melt-depleted lenses. Band spacing decreases and band width increases with decreasing shear stress. The vertical black cracks form at the end of an experiment as the sample is cooled to room temperature; they develop in response to the difference between thermal contraction of the sample and that of the tungsten pistons. The groves along the top and bottom of the sample, which were formed as serrations in the pistons pressed into the partially molten aggregate, have a spacing of ∼250 μm. Modified from Holtzman & Kohlstedt (2007).
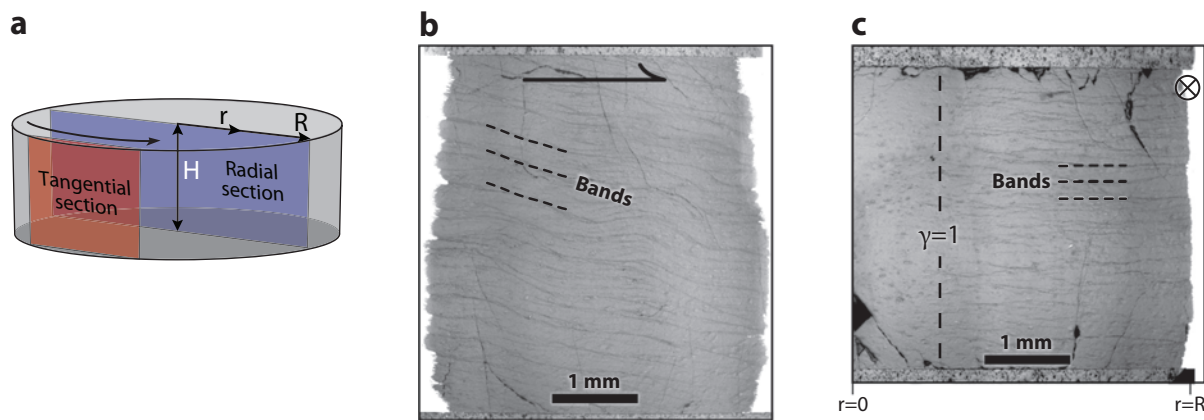


**Figure 7**

Sketch and two reflected optical micrographs of partially molten sample of olivine + 4 vol% MORB deformed in torsion. In (*a*), the tangential and radial cross sections are identified. In (*b*), melt-enriched bands (*dark streaks*) extend across the tangential section, back rotated to an angle of ∼20° to the shear plane. Shear direction is top to the right. In (*c*), melt-enriched bands extend horizontally from the edge ($r = R$) toward the center ($r = 0$) of the radial section, terminating at the point at which $\gamma \approx 1$. Shear direction is into the page for the right half of the sample.
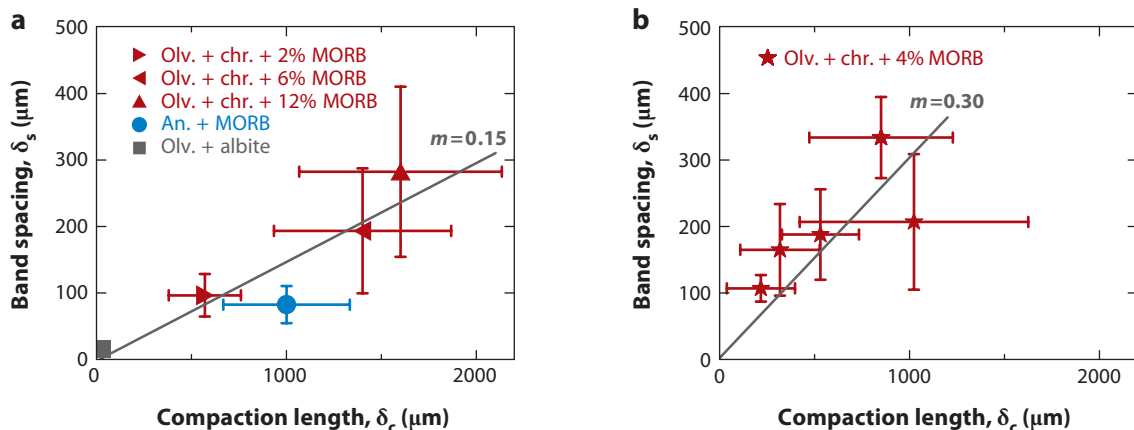
**Figure 8**

Band spacing, $\delta_s$, as a function of compaction length, $\delta_c$. (*a*) The triangular solid symbols are the olivine + chromite + MORB samples, with melt volumes listed in the legend. The vertical error bars are the standard deviations in the data. The linear best fit has a slope of $m = 0.15$. Modified from Holtzman et al. (2003a). (*b*) Data from samples of olivine + chromite + 4 vol% MORB deformed at a series of different stresses. The slope of a linear fit to the data is $m = 0.3$. Modified from Holtzman & Kohlstedt (2007). The difference in slope between the two studies (0.15 and 0.3) is likely due to the difference in methods used for calculating the compaction length, as required by the experimental designs.

**Compaction length scaling.** Compaction length is a useful concept for estimating both the occurrence of stress-driven spontaneous segregation and the spacing of bands within the sample (Holtzman et al. 2003a, Holtzman & Kohlstedt 2007). In direct shear experiments in which compaction length was varied by systematically changing viscosity of the partially molten rock, melt viscosity, and permeability, melt segregated into melt-enriched bands in samples that had initial compaction lengths less than or on the order of the sample thickness. Although melt pockets aligned at ~20° to the shear plane, melt segregation did not occur in samples with compaction lengths much larger than the sample thickness, presumably because melt flowed quickly enough that internal pressure gradients could not be sustained. Importantly, in these experiments, the spacing between the widest bands is proportional to the compaction length, as shown in **Figure 8a**.

In a second series of direct shear experiments, we varied compaction length by varying the applied stress (Holtzman & Kohlstedt 2007). The stress-driven melt segregation microstructures produced in three samples, each deformed at a different shear stress, are compared in **Figure 6**. Because olivine deformed near the boundary between dislocation creep and diffusion creep, an increase in applied stress drove the material further into the non-Newtonian dislocation creep field. In this creep regime, the viscosity decreases with increasing stress according to the relation $\eta \propto \tau^{(1-n)}$, where $\tau$ is the shear stress and $n = 3$–4 is the stress exponent. Thus, viscosity of the partially molten sample was reduced by increasing the applied stress without changing permeability or fluid viscosity. The spacing between the largest bands increases with increasing compaction length, as plotted in **Figure 8b**; the sample deformed at the lowest stress has the largest compaction length and thus the largest spacing between melt-enriched bands. The slope of this plot of band spacing versus compaction length is about a factor of two larger than that calculated from the data in **Figure 8a**, largely because of the different methods used to calculate viscosity and thus compaction length in the two studies.

Once melt segregation occurs, the compaction length varies over a length scale smaller than the original value for the homogeneous melt distribution and thus loses meaning as an average value of the system. This situation arises because of the strong dependence of compaction length on melt fraction, as illustrated in figure 7 of Holtzman et al. (2003a). Nonetheless, compaction length provides a relation between reference properties of the system that appears to be effective at predicting the occurrence of segregation and at indicating the steady-state length scale of melt segregation (the spacing between the largest bands) that a system will achieve.

## THEORETICAL CONSIDERATIONS RELATED TO SPONTANEOUS MELT SEGREGATION

Even though the microstructural patterns in these experiments are very complex, the boundary and thermodynamic conditions are simple relative to those in natural systems. As an approach to understanding the extrapolation from experiments to the Earth, theoretical models must be developed to describe behavior in experiments and then modified to apply to large-scale systems with chemical interactions, complex boundary conditions, and interplays of the driving forces for melt migration. In this section, we discuss current understanding in modeling of spontaneous segregation during deformation in the viscous regime, in the context of direct applications to experimental observations. Subsequently, we discuss modeling in a more complex natural setting.

As discussed above, the theoretical prediction of stress-driven segregation in deforming partially molten rocks (Stevenson 1989) preceded the experimental observation of this phenomenon (Holtzman et al. 2003a). However, this initial theoretical analysis did not provide a strong constraint on the wavelength of the instability, only suggesting that it would be smaller than the compaction length and larger than the grain size. This suggestion is consistent with experimental observations of a relationship between compaction length and maximum band spacing (Holtzman et al. 2003a). This result led to an attempt to describe the phenomenon with two-phase flow theory.

Spiegelman (2003) extended Stevenson's (1989) analysis from one-dimensional pure shear to two-dimensional simple shear, solving a linear stability analysis of band growth rate in a 2-D shear flow. He demonstrated that an instability would develop for a system with a Newtonian, melt fraction–dependent viscosity, but the growth rate in his analysis was highest for bands at 45° to the shear plane, normal to the direction of maximum tension, $\sigma_3$. A similar solution was found by Rabinowicz & Vigneresse (2004). The first-order implication of these results is that the porosity dependence of viscosity provides a nonlinearity to the problem that is required to cause segregation in simple shear, but it does not explain the ubiquitous occurrence in experimentally deformed samples of melt-enriched bands at ∼20° to the shear plane, antithetic to the shear direction.

Building on Spiegelman's (2003) analysis, Katz et al. (2006) explored another source of nonlinearity, namely the stress-dependence of the matrix viscosity, to test the possibility that this effect could stabilize bands at a lower angle to the shear plane. Both a linear stability analysis and fully nonlinear numerical models demonstrated that a non-Newtonian (stress-dependent) viscosity does indeed stabilize melt-enriched bands at lower angles to the shear plane. The stress- or strain rate–dependence of viscosity leads to an additional feedback in the regions with elevated melt fraction because the effective viscosity is further reduced by the strain rate amplification in low-viscosity regions, enhancing decompaction in those regions and further enhancing strain partitioning. The resulting preferred angle of ∼20°, for a stress exponent of $n = 4$–6, reflects a balance of strain localization (which decreases the angle) and band growth (which is maximum at 45°). While band

angles obtained from this model are in good statistical agreement with experimental observations, the model predicts a dependence of band angle on the stress exponent $n$. In experiments, band angles do not appear to depend on $n$, which varies from approximately 1 to 4, reflecting the variable contributions of diffusion and dislocation creep. This discordance between model and experiment suggests that the essential element in reducing the angle between melt-enriched bands and the shear plane is the enhancement of strain rate in the bands; the dependence of viscosity on stress can be an important contributor to this localization, but other mechanisms could also be important.

Takei & Holtzman (2009a,b,c) explored another type of nonlinearity resulting from a stress-induced microstructural change at the grain scale. To approach the multiscale problem ranging from melt alignment at the grain scale to melt segregation and organization over distances greater than the grain scale, they introduced into two-phase flow theory an internal state variable, contiguity (Takei 1998), that describes the melt topology. The detailed grain-scale, three-dimensional melt distribution can be characterized with this state variable, thus providing more information than melt fraction alone. To build a more complete theoretical formulation, it is important to consider (*a*) the physical processes controlling the evolution of the melt distribution or contiguity, specifically, the driving force and mechanism for stress-induced alignment of melt at the grain scale and (*b*) the sensitivity of viscosity of a partially molten rock to changes in contiguity.

To address the first question, Hier-Majumder et al. (2004) analyzed the thermodynamics and kinetics of melt alignment in response to an applied shear stress. They explored wetting of favorably oriented grain boundaries under the influence of an external applied shear stress. In this analysis, the localized tensile stress concentration at solid-solid-liquid junctions is relaxed through wetting of appropriately oriented grain boundaries by diffusive flow of melt from a triple junction into the initially dry portion of the grain boundaries to produce an anisotropic network of melt, as illustrated in **Figure 5**. Takei & Holtzman (2009b) showed that asymmetry in the distribution of melt around a grain can develop due to the effects of deviatoric stress on melt composition. Both processes lead to anisotropic melt topologies not present under hydrostatic conditions.

To address the second question, a grain-scale model was developed to understand the effects of a three-dimensional distribution of melt on the constitutive relations for grain-boundary diffusion creep (Takei & Holtzman 2007b, 2009a). This model, which was built on the geometric basis used to investigate the effects of melt on elastic properties (Takei 1998), demonstrates that anisotropic viscosity that develops as a result of anisotropic contiguity causes a coupling between the shear and normal components of the stress tensor. This coupling influences segregation and organization of melt at a macroscopic scale and results in a maximum in growth rate of melt-enriched bands at an angle similar to that observed in experiments. In other words, an applied shear stress causes alignment of pockets and grain-scale anisotropic viscosity, which lead to the development of pressure perturbations that then result in segregation instability. Thus, processes and properties at the grain scale lead to organization at larger length scales.

The effects of segregated multiscale melt organization on the effective viscosity of a partially molten rock are yet to be well-quantified in experiments, but constraints exist from simple models (e.g., Takei & Holtzman 2009c). Strain partitioning between networks of melt-enriched bands and melt-depleted lenses is another nonlinear coupling that can influence the band angle as well as macroscopic deformation behavior. To explore this interaction, Holtzman et al. (2005) calculated steady-state energy dissipation of a system in which deformation is partitioned between two regions of contrasting viscosities. Their analysis reveals that strain partitioning between melt-enriched bands and melt-depleted lenses necessitates a coupling in the velocity fields in the two regions, which leads to a back-rotation of the shear planes and hence of olivine b-planes, as observed in experiments and discussed below. The band angle is associated with a minimum in the rate of viscous energy dissipation or rate of entropy production of the composite material, which occurs

when strain rates are ideally partitioned between the two regions in accord with their viscosity ratio. This minimization was not an assumption but a consequence of the model. This condition also coincides with that in which the magnitude of the shear stress is the same in the melt-enriched bands and the melt-depleted lenses. Small deviations from this ideal configuration cause local pressure gradients that drive melt reorganization during deformation, allowing a statistical steady-state melt topology. Such coupling is also discussed by Spiegelman (2003) and observed in the numerical experiments of Katz et al. (2006).

In summary, the dependence of viscosity on melt fraction leads to an instability in melt distribution (Stevenson 1989). In simple shear, two-phase flow theory predicts that bands at 45° to the shear plane grow fastest if the dependence of viscosity on melt fraction is the only effect of coupling melt distribution and deformation (Spiegelman 2003, Rabinowicz & Vigneresse 2004, Katz et al. 2006, Takei & Holtzman 2009c). This effect alone does not provide enough nonlinear coupling to explain the observed 20° angle. Other sources of coupling that reduce the band angles are (*a*) a nonlinear stress dependence of viscosity (Katz et al. 2006), (*b*) anisotropic viscosity due to stress-induced anisotropic melt distribution at the grain scale (Takei & Holtzman 2007b, 2008a), and (*c*) the coupling between bands and lenses during strain partitioning (Holtzman et al. 2005). Other possible sources for nonlinearity include (*a*) the relationship between melt fraction and the kinetics of grain growth and grain size reduction, (*b*) effects of elastic anisotropy due to LPO development, and (*c*) shear-induced granular flow completely balanced by decompaction (i.e., grain-switching in the melt-rich regions that is partly accommodated by grain deformation and partly by pore-volume increase coupled with local melt migration). The relative importance of these various processes in the formation and orientation of melt-enriched bands has yet to be considered. Although significant progress has been made recently in understanding the influences of deformation on melt distribution, a model completely consistent with experimental observations has not yet emerged.

## INFLUENCE OF MELT DISTRIBUTION ON ROCK TEXTURE

The effect of melt distribution on the lattice preferred orientation (LPO) in sheared partially molten samples provides insight into the mechanisms of high-temperature plastic deformation active during segregation and organization of melt. One test of the applicability of results from laboratory experiments to processes occurring deep in the Earth is similarity of microstructures and LPO. In the context of the present review, LPO provides a clear indication of pervasive partitioning of strain between the melt-depleted lenses and the network of melt-enriched bands.

Examination of the LPO of samples of melt-free olivine provides a reference point for analyzing the LPO of sheared partially molten samples. Pole figures obtained in our laboratory on deformed samples of melt-free olivine are in excellent agreement with those published by other groups. The pole figures in **Figure 9a** for a sample deformed in direct shear (**Figure 3c**) match those reported by Zhang & Karato (1995). Likewise, the pole figures in **Figure 9b** for a sample of melt-free olivine deformed in torsional shear (**Figure 3d**) agree well with results from Bystricky et al. (2000). The fabric produced in torsional shear differs somewhat from that obtained in direct shear experiments, as illustrated by comparing **Figure 9b** with **Figure 9a**. This difference arises because the compressional stress intrinsic to deformation in the direct shear geometry assists in rotating the slip planes in the olivine grains toward the shear plane (Tommasi et al. 1999).

Two fundamental observations are persistent in a comparison of pole figures of melt-free olivine with those obtained from melt-bearing samples in which the melt phase has segregated into melt-enriched bands (Holtzman et al. 2003b). First, relative to the LPO produced in melt-free olivine samples during direct shear experiments (**Figure 9a**), the b-planes of olivine in the melt-depleted
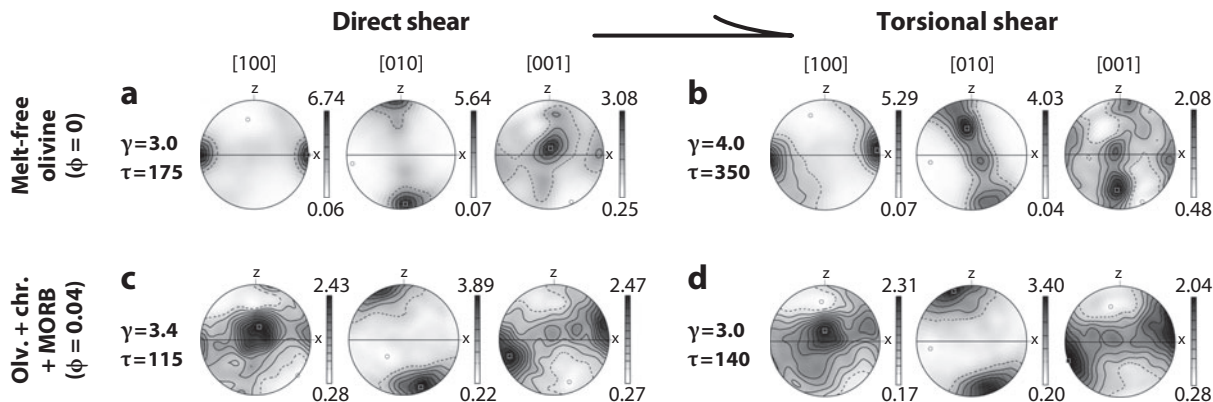
**Figure 9**

Lattice preferred orientation of samples of melt-free olivine and olivine + chromite + MORB deformed in direct shear and in torsional shear at the shear stresses, τ, to the shear strains, γ, indicated. (*a*) Pole figures for sample of melt-free olivine deformed in direct shear. (*b*) Pole figures for sample of melt-free olivine deformed in torsional shear. (*c*) Pole figures for sample of olivine + chromite + 4 vol% MORB deformed in direct shear. (*d*) Pole figures for sample of olivine + chromite + 4 vol% MORB deformed in torsional shear. Each pole figure is a lower hemisphere equal-area projection. The sense of shear is indicated by the arrow. The scale bar and numbers to the right of each pole figure correspond to multiples of uniform distribution. Implications of these fabrics are discussed in detail in the text.

lenses are back rotated by ∼20° to the shear plane if melt is present, aligned, and segregated (**Figure 9*c***). This angle is approximately equal in magnitude but opposite in sign to the angle between the melt-enriched bands and the shear plane. This back rotation is the consequence of strain partitioning, which permits strain on melt-enriched bands at ∼20° to be compensated by strain in the melt-depleted lenses on back-rotated slip planes such that the two volume-weighted strains sum to the total strain imposed on the sample (Holtzman et al. 2005).

Second, the ubiquitous a-axis alignment in the shear direction (shear-a-parallel) reported for melt-free samples deformed at high temperature (**Figure 9*a,b***) breaks down in the presence of melt, particularly in sheared samples with networks of melt-enriched bands. In partially molten samples, the concentration of aligned a-axes is a factor of 2 to 3 smaller than in melt-free samples. In addition the a-axes of olivine grains are aligned predominantly normal to the shear direction rather than parallel to the shear direction (as shown in **Figure 9*c,d***). This change was previously referred to as the "a-c switch" and here is called "shear-a-normal." This observation is highly reproducible. In samples of olivine + chromite + MORB, the shear-a-normal fabric develops not only in the transpressional deformation of direct shear experiments (**Figure 9*c***) but also in the simple shear deformation of torsional shear (**Figure 9*d***), meaning that the component of stress normal to the shear plane is not an essential part of the transition from shear-a-parallel to shear-a-normal fabric.

The usual interpretation of the shear-a-normal fabric is that slip in the [001] direction is active. However, there is no mechanistic reason to argue that the presence of melt activates glide of dislocations with [001] slip vectors in preference to dislocation with [100] slip vectors. Furthermore, the shear-a-normal fabric cannot be caused by the presence of relatively strong chromite grains because the same fabric develops in samples of olivine + MORB (F. Heidelbach, unpublished data) and samples of olivine + molten FeS + MORB (Holtzman et al. 2003b). Instead, we propose that the shear-a-normal fabric is a consequence of strain partitioning in deforming partially molten rocks. At the scale of melt-enriched bands, melt segregation must cause strain to partition between regions within a rock, specifically, melt-enriched bands and melt-depleted lenses. At the scale of the grain size, melt alignment must cause strain to partition

between deformation mechanisms (diffusion creep, grain boundary sliding, and dislocation creep) in an anisotropic manner such that the relative contribution of each mechanism depends on direction in the sample. Anisotropic partitioning of strain causes local modifications in the stress state. For example, deformation in the shear plane in the shear direction may be preferentially accommodated by melt-assisted grain boundary diffusion creep, causing local shear stresses on grain-to-grain contacts to enhance out-of-plane stresses, reducing the a-axis alignment in the shear direction. Although this process is not understood in detail, it is likely to occur in a system that is deforming in which diffusion and dislocation creep are both contributing significantly to the total strain rate. Since deformation in the asthenosphere is likely to be occurring near this boundary (de Bresser et al. 2001, Hirth & Kohlstedt 2003), these melt-sensitive processes affecting the LPO may be relevant to the interpretation of seismic anisotropy.

Based on the shear-a-normal fabrics produced in direct shear experiments on partially molten samples, the relevance of these results to the Earth has been questioned as an "experimental artifact" that "does not apply to natural settings" (Karato et al. 2007). This statement is both misleading and incorrect. First, the artifact to which they are referring, the compressional component in direct shear, is not an experimental artifact; rather, it is a boundary condition that influences the process being studied, which is ubiquitous in and relevant to natural settings. Second, the fact that the shear-a-normal fabric produced in samples deformed in direct shear is also observed in samples deformed in torsion means that the influence of the compressional component is not an essential part of the process of producing this fabric.

## APPLICATION TO EARTH

Building on the experimentalist's perspective, we discuss the influence of deformation on the ensemble of processes that contribute to melt extraction from the mantle. By design, experiments impose simple boundary conditions on systems with systematic changes in as few variables as possible in order to understand the influence of each variable on the behavior of that system. Natural systems generally involve complex boundary conditions and experience evolving loading and thermodynamic paths with many of the internal variables changing simultaneously. Above we discussed modeling efforts undertaken to understand the behavior observed in experiments (Spiegelman 2003, Katz et al. 2006, Takei & Holtzman 2009c). Here our goal is to motivate inquiries that are best explored by mathematical modeling as a bridge between the simple and the complex, using experimental observations as benchmarks. In the following sections, we address first the scaling of basic properties of partially molten rocks from laboratory to earth conditions. We then return to **Figure 1** to discuss the scaling relations in the context of a simple picture of the distribution of these properties in one geodynamic setting.

## Scaling from Laboratory to Earth

Due to constraints on the lifetime of an experimentalist, laboratory deformation experiments must be carried out at strain rates that are fast compared to those appropriate for flow processes in the mantle ($10^{-4}$–$10^{-6}$ s$^{-1}$ versus $10^{-12}$–$10^{-14}$ s$^{-1}$). To work at laboratory strain rates, experiments are generally performed at differential stresses higher than those found in the mantle (3–300 MPa versus 0.1–1 MPa). Also, for samples to reach textural equilibrium or attain a steady-state microstructure in the laboratory environment, fine-grained (grain size $d \approx 10$ μm) samples are often used so that diffusion distances are relatively short. Ultimately, it is necessary to scale laboratory results to mantle conditions. In the following discussion, we focus on the extrapolation of

experimental results on the influences of stress on melt distribution, beginning with processes at the grain scale and building upward.

**Is stress in the asthenosphere large enough to align and segregate melt?** In shear deformation experiments (Holtzman et al. 2003a), melt migration, segregation, and organization are driven by gradients in mean stress associated with regional variations in viscosity (Stevenson 1989) and resisted by pressure gradients due to gradients in surface tension (Stevenson 1986, Riley & Kohlstedt 1991). The fact that segregation occurs demonstrates that differential stress dominates over surface tension. Recent experiments demonstrate that the kinetics of surface tension-driven homogenization of melt is demonstrably slower in the lab than stress-driven segregation of melt (Parsons et al. 2008). In the asthenosphere, stress should dominate over surface tension such that stress-driven melt segregation can occur (Cooper & Kohlstedt 1984, 1986; Holtzman & Kohlstedt 2007).

Two important dimensionless numbers must be considered in discussing extrapolation of laboratory results to conditions in the asthenosphere (D. Stevenson, personal communication). The first is a nondimensional thermodynamic parameter, $\sigma/(\Gamma/r_c)$, which is the ratio of the differential stress, $\sigma$, to the surface tension expressed as the surface energy, $\Gamma$, divided by the radius of curvature of the melt pocket, $r_c$. In laboratory experiments, surface tension, $\Gamma/r_c \approx 3\Gamma/d\phi^{1/2} \approx 1$ MPa, is relatively large, where $d = 15$ μm, $\phi = 0.04$, and $\Gamma = 1$ J/m$^2$ (Cooper & Kohlstedt 1982). In the asthenosphere with $d = 3$ mm and $\phi = 0.01$, $\Gamma/r_c \approx 0.01$ MPa. Thus, in both the lab and the upwelling mantle, the nondimensional thermodynamic driving force $\sigma/(\Gamma/r_c)$ is larger than unity, such that differential stress dominates over surface tension in both cases. This condition is necessary, though not sufficient, for textural change to be produced by deformation of a partially molten rock.

The second quantity is a nondimensional kinetic parameter, $\dot{\varepsilon}/(cD/d^2)$, the ratio of the strain rate, $\dot{\varepsilon}$, to the diffusive flux (where $c$ is the concentration and $D$ is the diffusivity of the slowest diffusing component of the solid in the melt). This parameter compares the rate at which the fluid pockets are distorted due to deformation to the rate at which they recover their shape as dictated by surface tension. Although $D$ and $c$ are similar in the lab and mantle, $\dot{\varepsilon}$ in the lab is about six to eight orders of magnitude larger than in the mantle, whereas $d^2$ is about five to six orders of magnitude larger in the mantle than in experiments. Hence the value of the kinetic parameter is approximately the same order of magnitude in the lab as it is in the upwelling mantle, and both are significantly larger than unity so that re-equilibration of the texture by diffusion processes does not destroy that formed by straining the rock. In this description, for the fluid pocket to recover its shape, the matrix grains must also deform to avoid opening of void space; that is, the problem involves two-phase flow requiring movement of both solid and fluid.

## Relations Between Melt-Extraction Mechanisms

To return to the framework developed in the Introduction, we summarize the relative contributions to the mechanism of spontaneous segregation of melt of (*a*) pressure gradients induced by buoyancy versus stress, (*b*) mechanical response by brittle versus viscous mechanisms, and (*c*) advective flow versus reactive infiltration. (*a*) and (*b*) correspond to the axes of the melt-migration mechanism map in **Figure 1**, and (*c*) describes the reactive infiltration instability. We use three dimensionless numbers to describe the relative contributions in each case.

**Stress versus buoyancy driving forces for melt migration (Φg number).** The question of the nature of the relative importance of buoyancy-driven melt migration and stress-driven

segregation remains open. Recent modeling studies have addressed this question in a geodynamic context (Butler 2009; K. Müller & H. Schmeling, manuscript submitted 2008). In the mantle, melt migrates in response to two distinct driving forces, given that surface tension is not important at the scale of a terrestrial planet. The pressure gradient due to buoyancy is $\Delta\rho g \approx$ 3 kPa/m, where $g$ is the acceleration due to gravity and $\Delta\rho \approx 300$ kg/m$^3$ is the difference between the density of the solid and that of the melt. The stress-induced pressure gradient in the melt phase resulting from local perturbations (over distances $<\delta_c$) in melt fraction is on the order of $\eta\dot\varepsilon/(0.3\delta_c) \approx 3$ kPa/m, where $\eta \approx 1 \times 10^{19}$ Pa s, $\dot\varepsilon \approx 1 \times 10^{-13}$ s$^{-1}$, and $\delta_c \approx 1$ km (Stevenson 1989). The relative importance of pressure gradients arising from buoyancy and stress can be described with the $\Phi g$ number (pronounced "Fiji"), which was defined by Phipps Morgan & Holtzman (2005) for vug waves. Here, we recast it in terms of a simple estimate for mean stress-driven versus buoyancy-driven segregation. A third driving force can arise due to dynamic pressure gradients at the scale of a mid-ocean ridge or a subduction zone, as discussed by Phipps Morgan (1987) and Spiegelman & McKenzie (1987), but it is not incorporated into the $\Phi g$ number here.

**Elastic versus viscous rheological responses to melt migration (Deborah number).** The Deborah number was defined above in Equations 2a and 2b. In laboratory experiments, $De \approx 10^{-4}$– $10^{-2}$ for deformation occurring in the viscous regime. In the asthenosphere, $De$ will vary spatially but is small enough to ensure that deformation of partially molten rocks occurs predominantly by viscous rather than brittle processes. A transition occurs to more brittle behavior as melt passes from the asthenosphere into the lithosphere.

**Reaction versus stress-driven melt segregation (Damköhler number).** The interplay between stress-driven segregation and reaction-driven segregation has not yet been studied. The Damköhler number is the ratio of the advection time to the reaction time in a volume of reacting solid and fluid, or alternatively, the ratio of a system length scale to a length scale of equilibration between fluid and solid (e.g., Aharonov et al. 1995). It is defined as $Da = (RAL)/(\phi\omega\rho_f)$ or $Da = L/L_{eq}$, where $L_{eq} = (\phi\omega\rho_f)/RA$, with $R$ the reaction rate constant, $A$ the specific surface area available for reaction, $L$ the system length scale, $\omega$ the melt velocity, and $\rho_f$ the fluid density. In a system with a solubility gradient (such as upwelling mantle beneath a mid-ocean ridge), a high value of $Da$ can lead to a reaction infiltration instability (Aharonov et al. 1995), as discussed in the Historical Background section. The dissolution or reaction rate is defined as $k_+ = -RA(c - c_{eq})$, where $(c - c_{eq})$ is the distance from the equilibrium concentration of any chemical species (i.e., the chemical driving force or affinity). Stress-driven segregation could affect all three of the factors in the dissolution rate, as discussed further below.

# APPLICATION TO A SIMPLE MID-OCEAN RIDGE SETTING

In **Figure 10a**, we illustrate the hypothesis that the lithosphere-asthenosphere boundary (LAB) beneath a mid-ocean ridge is characterized by networks of melt-enriched channels (Holtzman et al. 2005; Holtzman & Kohlstedt 2007; B.K. Holtzman & J.-M. Kendall, manuscript submitted 2008). The mechanical interface between the lithosphere and the asthenosphere may be characterized by a significant gradient in melt fraction, as discussed for the subcontinental LAB by Rychert et al. (2007). If melt is organized into melt-enriched shear zones on the LAB interface, the effective viscosity of that region will be significantly reduced relative to the effective viscosity of a region with the same melt fraction but with the melt homogeneously distributed. Thus, the mechanical lithosphere begins where the melt fraction decreases dramatically, because melting has two major

**a**

**b**

Strain rate

**c**

Φg number

**d**

Deborah number

**e**

Damköhler number

**f**
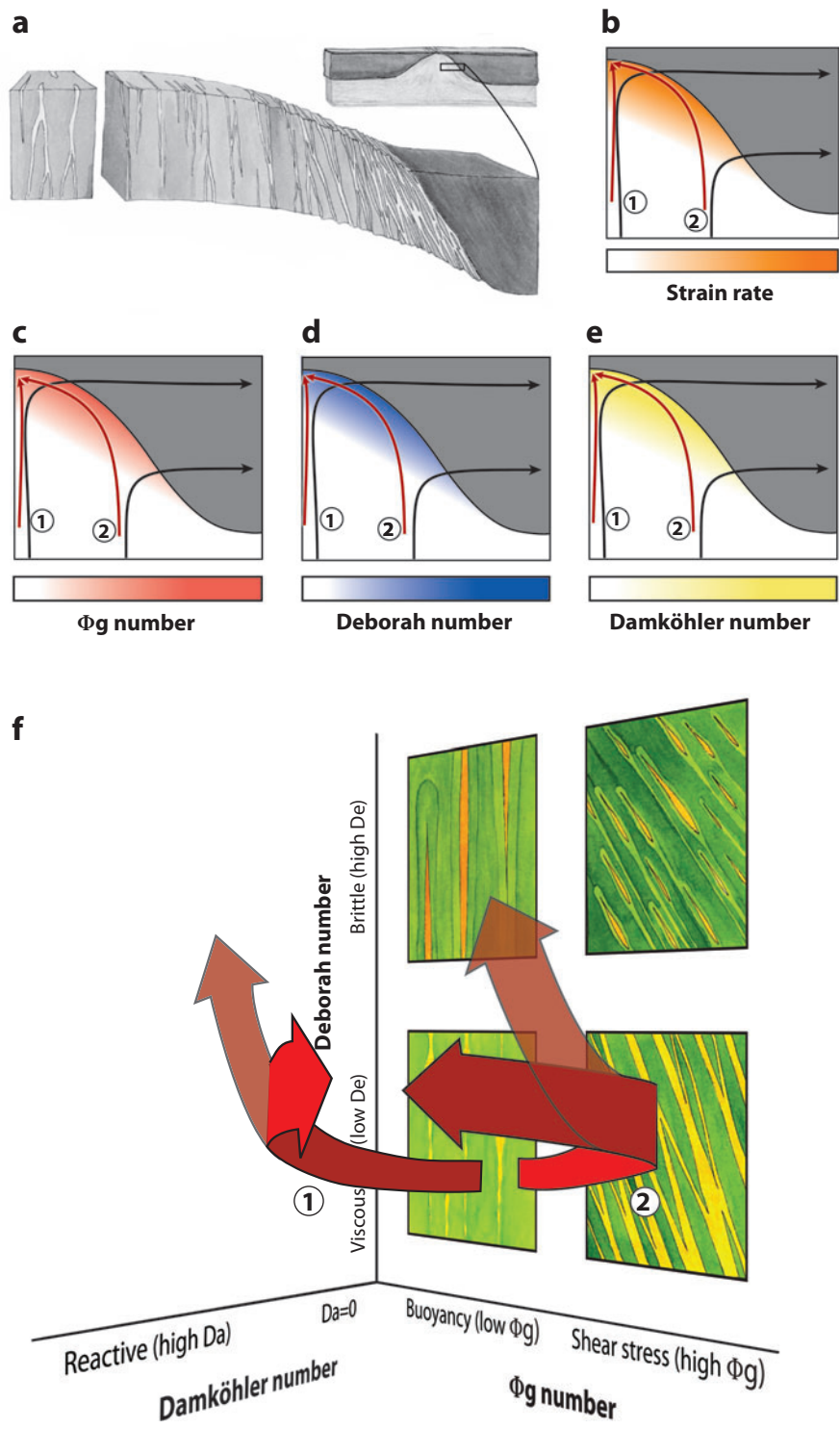
effects on rock strength: (*a*) the direct effect of enhancing creep rates and reducing viscosity and (*b*) the compositional effects of reducing water and iron content in the residue that increase its viscosity (Hirth & Kohlstedt 1996, Phipps Morgan 1997). If melt segregates and organizes most effectively where strain rates are highest, an effective lubrication of the plate boundary would occur. If the LAB is characterized by a melt-fraction gradient, then its location depends on the melt budget and may or may not correspond to a particular isotherm.

Spatial gradients in strain rate exist in the asthenosphere beneath a ridge axis during steady-state passive upwelling (e.g., Phipps Morgan 1987, Katz et al. 2006) as illustrated in **Figure 10*b***. Therefore, spatial gradients should also exist in the three scaling parameters discussed above, *De*, $\Phi$g, and *Da*, as illustrated in **Figure 10*c,d,e***. Here we keep the discussion qualitative, only indicating hypothetical directions of these gradients in the asthenosphere. $\Phi$g will increase in regions of high strain rate, while the buoyancy driving force is constant. The Deborah number will also increase as strain rate increases toward the LAB, but this increase may be offset in the asthenosphere by increasing melt fraction, which reduces viscosity. However, *De* will increase quickly in the adjacent lithosphere as melt fraction decreases. In locations where melt travels through high-permeability melt-enriched networks produced by stress-driven segregation (as opposed to dissolution- or reaction-driven segregation), the potential for melt-rock disequilibrium increases because melt flux can be enhanced without melt-rock reaction. In such a system in which solubility increases upward, two competing tendencies will be at play: Higher melt velocities will increase the degree of melt-rock disequilibrium, but the greater degree of disequilibrium will enhance dissolution rates. This competition is not explicitly described (yet) by the Damköhler number, because it does not contain the degree of disequilibrium. For example, increased melt velocity will decrease *Da*; increased surface area available for reaction will increase *Da*; increased distance from equilibrium will increase the dissolution rate (not expressed in *Da*, as currently formulated). For the sake of simplicity and raising questions, we suppose that *Da* increases as melt migrates upward in the system. Therefore, we expect stress to influence the form of dunite channels more toward the flanks of the melt-enriched region than in the center (as illustrated in **Figure 10*a*** and in figure 25 of Holtzman & Kohlstedt 2007, after Braun & Kelemen 2002). We also expect melts with greater degrees of disequilibrium to come more from the flanks than from the center of the subridge asthenosphere.

---

**Figure 10**

An exercise in extrapolation of melt-segregation mechanisms to a simple ridge setting. (*a*) A hypothetical gradient in melt distribution at the lithosphere-asthenosphere boundary (LAB), in which strain rate and thus the degree of stress-driven segregation and organization increase toward the LAB. The lithosphere is then comprised of the melt-depleted residual mantle material, and the position of the LAB depends on the melt budget. In the middle of the upwelling region, where strain rates are lowest, reaction-driven channel formation may dominate. (*b*) A map of strain rate increase due to passive corner flow, relative to a background level. Dark gray represents the lithosphere in which there is less, but more organized, deformation than in asthenosphere. (*c*) $\Phi$g increases with increasing strain rate. (*d*) *De* increases with increasing strain rate. (*e*) *Da* should increase with increasing strain rate if melt organizes due to stress-driven segregation, creating high-permeability pathways that enable melt-rock disequilibrium to increase at progressively higher levels in the system, because reaction rate kinetics will be enhanced by greater disequilibrium. (*f*) The melt-migration mechanism map from **Figure 1** is modified to include a third axis for the *Da* number. The dominant melt-migration mechanism, corresponding to a certain value of $\Phi$g, *Da*, and *De*, will change in pressure-temperature space, such that the melt migrating toward the surface will move through this space. The two examples of melt transport paths in the subridge asthenosphere (*1*) and (*2*) in (*b–e*) are shown as red arrows in (*f*) and discussed in the text. The transparent branches diverge toward transitional viscous-brittle processes higher up in the system.

The possible physical meaning of these variations in the three scaling parameters can be expressed in the melt-migration mechanism map in **Figure 1**, extended in **Figure 10f** to include a third axis representing the Damköhler number. For the two melt transport paths 1 and 2 shown in **Figure 10b–e**, we draw schematic arrows of the movement of melt by different migration mechanisms. Melt migrating up path 1 would progress to higher $Da$ before increasing in $\Phi g$. Therefore, the path may be characterized by greater reactive infiltration without much stress-driven segregation. Melt migrating up path 2 would progress to elevated values of $\Phi g$ followed by increasing $Da$. Thus it would enter a regime in which stress-driven organization develops quickly, as migrating melt approaches the LAB, and then subsequently reactive processes would interact with the deformation processes as the melt migrates along the LAB. The existence of this path is supported by geological evidence in the Lherz massif (Le Roux et al. 2008) and in the Lanzo massif (Kaczmarek & Müntener 2008). Reaction-driven or stress-driven instabilities in the viscous regime may evolve into transitional viscous-brittle-reactive processes. As melt leaves the asthenosphere, it makes a steep turn to higher $De$ and enters buoyancy-driven fractures (dikes) or shear stress-driven cracks (vug waves). $Da$, $De$, and $\Phi g$ will all change with pressure, temperature, grain size, and composition, as well as with the strain rate effects discussed above. Here, we present these paths not as definitive models but to provoke questions that will stimulate the integration of mechanical, kinetic, and compositional constraints on melt migration and extraction processes. This approach can be taken for any planetary setting, including lower continental crust, mid-ocean ridges, subduction zones, plumes, and the core-mantle boundary.

## SUMMARY POINTS

1. Extraction of melt from Earth's mantle involves buoyancy-driven flow through channels formed by brittle fracture at low temperatures and by melt-solid reaction and/or stress-driven melt segregation at high temperatures.

2. Shear deformation experiments on partially molten rocks in the viscous regime demonstrate that a melt-preferred orientation develops at the grain scale and melt segregation into a network of melt-enriched bands occurs at a larger scale. Both the grain-scale melt pockets and the larger-scale melt-enriched bands are oriented ~20° to the shear plane, antithetic to the shear direction.

3. The spacing between melt-enriched bands increases systematically with increasing compaction length with a proportionality factor of 1/6 to 1/3 in laboratory deformation experiments.

4. Theoretical models of spontaneous melt segregation during shear deformation of partially molten rocks are based on the dependence of rock viscosity on melt fraction, the dependence of matrix viscosity on stress (non-Newtonian viscosity), strain partitioning between melt-enriched bands and melt-depleted lenses, and the anisotropy in viscosity arising from grain-scale melt alignment.

5. The lattice preferred orientation of partially molten rocks sheared to large strain is distinctly different from that of deformed melt-free samples. If melt is added, the ubiquitous shear-a-parallel fabrics obtained for the latter are replaced by shear-a-normal fabrics with back-rotated slips planes, indicative of strain partitioning between melt-enriched and melt-depleted regions.

6. Scaling arguments indicate that results obtained from laboratory experiments on partially molten rocks are applicable to deformation in Earth's mantle.

7. In a passively upwelling plate-spreading environment, strain rates are highest in the zone of corner flow and increase toward the ridge axis. Based on the simple point that stress-driven melt segregation and organization will be most effective where strain rates are highest, we hypothesize that the LAB is marked by the location of melt-enriched shear zones that lubricate the LAB and thus the plate boundary system. If melt moves rapidly through these networks formed initially at depth by a mechanical rather than reaction-driven instability, then the LAB should be the location of greatest melt-rock disequilibrium.

## FUTURE ISSUES

1. Melt-migration mechanisms. A number of issues remain related to the mechanisms of melt migration through and deformation of partially molten rocks in both laboratory experiments and theoretical analyses. For example, distinctions between chemical and mechanical processes are artificial. These two approaches to investigating the behavior of partially molten rocks need to be combined in order to proceed toward a more complete thermodynamical description. Some aspects of reaction-driven instabilities are well understood, but open questions remain as to their application to natural systems. Formation of melt-enriched channels by melt-solid reaction and those formed during deformation are likely to be closely coupled under some conditions, resulting in nonlinear behavior that has not yet been explored.

2. Melt distribution, deformation mechanisms, and rheological behavior. Many interesting aspects of the processes that govern rock deformation near the solidus are poorly understood. This paper was framed with the notion that the effects of melt fraction on viscosity are relatively well understood, but the effects of deformation on melt distribution are not. The symmetry in these two approaches implies that interactions and feedbacks exist among melt distribution and viscosity and stress during deformation that are only beginning to be studied. For example, we have demonstrated that melt strongly influences LPO, but we have not addressed the influence of LPO on the melt distribution. The extent to which segregation, organization, and strain partitioning influence the rheological properties of partially molten rocks, over multiple length and time scales, has not been fully resolved.

3. Extrapolation to Earth. The extrapolation of the understanding gained from experiments requires models to explore the interactions of driving forces and open system behavior that cannot be studied in experiment, at appropriate length and time scales and boundary conditions. Segregation and organization of melt during deformation may have important consequences for geodynamics, through their influences on rheological and transport properties. We have discussed the hypothesis that stress-driven organization will contribute to both melt extraction and mechanical lubrication of plate boundaries.

While we consider these questions in the context of a simple ridge setting, it is possible that this ensemble of processes that couple fluid flow (not limited to melt) are important at all plate boundaries.

## DISCLOSURE STATEMENT

The authors are not aware of any biases that might be perceived as affecting the objectivity of this review.

## ACKNOWLEDGMENTS

## LITERATURE CITED

Aharonov E, Spiegelman M, Kelemen P. 1997. Three-dimensional flow and reaction in porous media; implications for the Earth's mantle and sedimentary basins. *J. Geophys. Res.* 102:14821–33

Aharonov E, Whitehead JA, Spiegelman M, Kelemen P. 1995. Channeling instability of upwelling melt in the mantle. *J. Geophys. Res.* 100:20433–50

Ahern JL, Turcotte DL. 1979. Magma migration beneath an ocean ridge. *Earth Planet. Sci. Lett.* 445:115–22

Bai Q, Jin Z-M, Green HW. 1997. Experimental investigation of the rheology of partially molten peridotite at upper mantle pressures and temperatures. In *Deformation-Enhanced Fluid Transport in the Earth's Crust and Mantle*, ed. MB Holness, pp. 40–61. London: Chapman & Hall

Beeman ML, Kohlstedt DL. 1993. Deformation of olivine-melt aggregates at high temperatures and confining pressures. *J. Geophys. Res.* 98:6443–52

Bésuelle P. 2001. Compacting and dilating shear bands in porous rock: Theoretical and experimental conditions. *J. Geophys. Res.* 106:13435–42

Braun MG, Kelemen PB. 2002. Dunite distribution in the Oman Ophiolite: implications for melt flux through porous dunite conduits. *Geochem. Geophys. Geosyst.* 3:8603

Bulau JR, Waff HS, Tyburczy JA. 1979. Mechanical and thermodynamic constraints on fluid distribution in partial melts. *J. Geophys. Res.* 84:6102–8

Bussod GY, Christie JM. 1991. Textural development and melt topology in spinel lherzolite experimentally deformed at hypersolidus conditions. *J. Petrol. Spec. Lherzolite Issue*, pp. 17–39

Butler SL. 2009. The effects of buoyancy on shear-induced melt bands in a compacting porous medium. *Earth Planet. Sci. Lett.* In press

Bystricky M, Kunze K, Burlini L, Burg J-P. 2000. High shear strain of olivine aggregates: Rheological and seismic consequences. *Science* 290:1564–67

Chadam J, Hoff D, Merino E, Ortoleva P, Sen A. 1986. Reactive infiltration instability. *J. Appl. Math.* 36:207–21

Cmíral M, Fitz Gerald JD, Faul UH, Green DH. 1998. A close look at dihedral angles and melt geometry in olivine-basalt aggregates: A TEM study. *Contrib. Mineral. Petrol.* 130:336–45

Connolly JAD, Podladchikov YY. 1998. Compaction-driven fluid flow in viscoelastic rock. *Geodin. Acta* 11:55–84

Connolly JAD, Podladchikov YY. 2007. Decompaction weakening and channeling instability in ductile porous media: Implications for asthenospheric melt segregation. *J. Geophys. Res.* 112:B10205

Cooper RF. 1990. Differential stress-induced melt migration: an experimental approach. *J. Geophys. Res.* 95:6979–92

Cooper RF, Kohlstedt DL. 1982. Interfacial energies in the olivine-basalt system. In *High-Pressure Research in Geophysics, Advances in Earth and Planetary Sciences*, ed. S Akimota, MH Manghnani, 12:217–28. Tokyo: Cent. Acad. Publ. 632 pp.

Cooper RF, Kohlstedt DL. 1984. Solution-precipitation enhanced creep of partially molten olivine-basalt aggregates during hot-pressing. *Tectonophysics* 107:207–33

Cooper RF, Kohlstedt DL. 1986. Rheology and structure of olivine-basalt partial melts. *J. Geophys. Res.* 91:9315–23

Cooper RF, Kohlstedt DL, Chyung CK. 1989. Solution-precipitation enhanced creep in solid-liquid aggregates which display a nonzero dihedral angle. *Acta Metall.* 37:1759–71

Daines MJ, Kohlstedt DL. 1993. A laboratory study of melt migration. *Philos. Trans. R. Soc. London Ser. A* 342:43–52

Daines MJ, Kohlstedt DL. 1994. The transition from porous to channelized flow due to melt/rock reaction during melt migration. *Geophys. Res. Lett.* 21:145–48

Daines MJ, Kohlstedt DL. 1997. Influence of deformation on melt topology in peridotites. *J. Geophys. Res.* 102:10257–71

de Bresser JHP, Ter Heege JH, Spiers CJ. 2001. Grain size reduction by dynamic recrystallization: can it result in major rheological weakening? *Int. J. Earth Sci.* 90:29–45

Drew DA. 1983. Mathematical modeling of two-phase flow. *Annu. Rev. Fluid Mech.* 15:261–91

Drury MR, Fitz Gerald JD. 1996. Grain boundary melt films in an experimentally deformed olivine-orthopyroxene rock: implications for melt distribution in upper mantle. *Geophys. Res. Lett.* 23:701–4

Faul UH. 1997. Permeability of partially molten upper mantle rocks from experiments and percolation theory. *J. Geophys. Res.* 102:10299–311

Faul UH, Fitz Gerald JD. 1999. Grain misorientations in partially molten olivine aggregates: an electron backscatter diffraction study. *Phys. Chem. Miner.* 26:187–97

Faul UH, Toomey DR, Waff HS. 1994. Intergranular basaltic melt is distributed in thin, elongated inclusions. *Geophys. Res. Lett.* 21:29–32

Fowler AC. 1985. A mathematical model of magma transport in the asthenosphere. *Geophys. Astrophys. Fluid Dynam.* 33:63–96

Fowler AC, Scott DR. 1996. Hydraulic crack propagation in a porous medium. *Geophys. J. Int.* 127:595–604

Gourlay CM, Dahle AK. 2007. Dilatant shear bands in solidifying metals. *Nature* 445:70–73

Hall CE, Parmentier EM. 2000. Spontaneous melt localization in a deforming solid with viscosity variations due to water weakening. *Geophys. Res. Lett.* 27:9–12

Hart SR. 1993. Equilibration during mantle melting: a fractal tree model. *Proc. Natl. Acad. Sci. USA* 90:11914–18

Hier-Majumder S, Leo PH, Kohlstedt DL. 2004. On grain boundary wetting during deformation. *Acta Mater.* 52:3425–33

Hirth G, Kohlstedt DL. 1995a. Experimental constraints on the dynamics of the partially molten upper mantle: deformation in the diffusion creep regime. *J. Geophys. Res.* 100:1981–2001

Hirth G, Kohlstedt DL. 1995b. Experimental constraints on the dynamics of the partially molten upper mantle: deformation in the dislocation creep regime. *J. Geophys. Res.* 100:15441–49

Hirth G, Kohlstedt DL. 1996. Water in the oceanic upper mantle: implications for rheology, melt extraction and evolution of the lithosphere. *Earth Planet. Sci. Lett.* 144:93–108

Hirth G, Kohlstedt DL. 2003. Rheology of the upper mantle and the mantle wedge: a view from the experimentalists. In *Inside the Subduction Factory*, ed. J Eiler, *Geophys. Monogr.* 138:83–105. Washington, DC: Am. Geophys. Union

Holness MB. 2006. Melt-solid dihedral angles of common minerals in natural rocks. *J. Petrol.* 47:791–800

Holtzman BK, Groebner NJ, Zimmerman ME, Ginsberg SB, Kohlstedt DL. 2003a. Stress-driven melt segregation in partially molten rocks. *Geochem. Geophys. Geosyst.* 4:8607

Holtzman BK, Kohlstedt DL. 2007. Stress-driven melt segregation and strain partitioning in partially molten rocks: the evolution of melt distribution. *J. Petrol.* 48:2379–406

Holtzman BK, Kohlstedt DL, Phipps Morgan J. 2005. Viscous energy dissipation and strain partitioning in partially molten rocks. *J. Petrol.* 46:2569–92

Holtzman BK, Kohlstedt DL, Zimmerman ME, Heidelbach F, Hiraga T, Hustoft J. 2003b. Melt segregation and strain partitioning: implications for seismic anisotropy and mantle flow. *Science* 301:1227–30

Hustoft JW, Kohlstedt DL. 2006. Metal-silicate segregation in deforming dunitic rocks. *Geochem. Geophys. Geosyst.* 7:Q02001

Jin ZM, Green HW, Zhou Y. 1994. Melt topology during dynamic partial melting of mantle peridotite. *Nature* 372:164–67

Johnson KTM, Dick HJB, Shimizu N. 1990. Melting in the oceanic upper mantle: an ion microprobe study of diopsides in abyssal peridotites. *J. Geophys. Res.* 95:2661–78

Kaczmarek M-A, Müntener O. 2008. Juxtaposition of melt impregnation and high-temperature shear zones in the upper mantle; field and petrological constraints from the Lanzo peridotite (Northern Italy). *J. Petrol.* doi:10.1093/petrology/egn065

Karato S-I, Jung H, Katayama I, Skemer P. 2007. Geodynamic significance of seismic anisotropy of the upper mantle: new insights from laboratory studies. *Annu. Rev. Earth Planet. Sci.* 36:59–95

Katz RF, Spiegelman M, Holtzman BK. 2006. The dynamics of melt and shear localization in partially molten aggregates. *Nature* 442:676–79

Kelemen PB, Dick HJB. 1995. Focused melt flow and localized deformation in the upper mantle: Juxtaposition of replacive dunite and ductile shear zones in the Josephine Peridotite, SW Oregon. *J. Geophys. Res.* 100:423–38

Kelemen PB, Hirth G, Shimizu N, Spiegelman M, Dick HJB. 1997. A review of melt migration processes in the adiabatically upwelling mantle beneath oceanic spreading ridges. *Philos. Trans. R. Soc. London Ser. A* 355:283–318

Kelemen PB, Shimizu N, Salters VJM. 1995. Extraction of mid-ocean-ridge basalt from the upwelling mantle by focused flow of melt in dunite channels. *Nature* 375:747–53

King DS, Kohlstedt DL, Zimmerman ME. 2007. Stress-driven melt segregation and shear localization in partially molten aggregates: experiments in torsion. *Eos Trans. AGU* 88(52) Fall Meet. Suppl., Abstr. T43D-07

Kohlstedt DL. 1992. Structure, rheology and permeability of partially molten rocks at low melt fractions. In *Mantle Flow and Melt Generation at Mid-Ocean Ridges*, ed. J Phipps Morgan, DK Blackman, JM Sinton, *Geophys. Monogr.* 71:103–21. Washington, DC: Am. Geophys. Union

Kohlstedt DL. 2007. Properties of rocks and minerals. Constitutive equations, rheological behavior, and viscosity of rocks. In *Treatise on Geophysics*, ed. G Schubert, 2.14:389–417. Oxford: Elsevier

Kohlstedt DL, Chopra PN. 1994. Influence of basaltic melt on the creep of polycrystalline olivine under hydrous conditions. In *Magmatic Systems*, ed. MP Ryan, pp. 37–53. New York: Academic. 401 pp.

Kohlstedt DL, Zimmerman ME. 1996. Rheology of partially molten mantle rocks. *Annu. Rev. Earth Planet. Sci.* 24:41–62

Le Roux V, Tommasi A, Vauchez A. 2008. Feedback between deformation and melt percolation in an exhumed lithosphere-asthenosphere boundary. *Earth Planet. Sci. Lett.* 274:401–13

Marone C. 1998. Laboratory-derived friction laws and their application to seismic faulting. *Annu. Rev. Earth Planet. Sci.* 26:643–96

McKenzie D. 1984. The generation and compaction of partially molten rock. *J. Petrol.* 25:713–65

Morgan ZT, Liang Y. 2005. An experimental study of the kinetics of lherzolite reactive dissolution with applications to melt channel formation. *Contrib. Mineral. Petrol.* 150:369–85

Nicolas A. 1986. A melt extraction model based on structural studies in mantle peridotites. *J. Petrol.* 27:999–1022

Nicolas A. 1989. *Structures of Ophiolites and Dynamics of Oceanic Lithosphere*. Dordrecht, The Netherlands: Kluwer Acad. 367 pp.

Ortoleva P, Chadam J, Merino E, Sen A. 1987. Geochemical self-organization II; the reactive-infiltration instability. *Am. J. Sci.* 287:1008–40

Parsons RA, Nimmo F, Hustoft JW, Holtzman BK, Kohlstedt DL. 2008. An experimental and numerical study of surface tension-driven melt flow. *Earth Planet. Sci. Lett.* 267:548–57

Paterson MS, Olgaard DL. 2000. Rock deformation tests to large shear strains in torsion. *J. Struct. Geol.* 22:1341–58

Phipps Morgan J. 1997. The generation of a compositional lithosphere by mid-ocean ridge melting and its effect on subsequent off-axis hotspot upwelling and melting. *Earth Planet. Sci. Lett.* 146:213–32

Phipps Morgan J. 1987. Melt migration beneath mid-ocean spreading centers. *Geophys. Res. Lett.* 14:1238–41

Phipps Morgan J, Holtzman BK. 2005. Vug waves: a mechanism for coupled rock deformation and fluid migration. *Geochem. Geophys. Geosyst.* 6:Q08002

Rabinowicz M, Vigneresse J-L. 2004. Melt segregation under compaction and shear channeling: application to granitic magma segregation in a continental crust. *J. Geophys. Res.* 109:B04407

Renner J, Viskupic K, Hirth G, Evans B. 2003. Melt extraction from partially motlen peridotites. *Geochem. Geophys. Geosyst.* 4:8606

Ribe NM. 1986. Melt segregation driven by dynamic forcing. *Geophys. Res. Lett.* 13:1462–65

Richardson CN, Lister JR, McKenzie D. 1996. Melt conduits in a viscous porous matrix. *J. Geophys. Res.* 101:20423–32

Richter FM, McKenzie D. 1984. Dynamical models for melt segregation from a deformable rock matrix. *J. Geol.* 92:729–40

Riley GN Jr, Kohlstedt DL. 1990. An experimental study of melt migration in an olivine-melt system. In *Magma Transport and Storage*, ed. MP Ryan, pp. 77–86. New York: Wiley

Riley GN Jr, Kohlstedt DL. 1991. Kinetics of melt migration in upper mantle-type rocks. *Earth Planet. Sci. Lett.* 105:500–21

Riley GN Jr, Kohlstedt DL, Richter FM. 1990. Melt migration in a silicate liquid-olivine system: an experimental test of compaction theory. *Geophys. Res. Lett.* 17:2101–4

Rosenberg CL, Handy MR. 2000. Synthectonic melt pathways during simple shearing of a partially molten rock analogue (norcamphor-benzamide). *J. Geophys. Res.* 105:3135–49

Rosenberg CL, Handy MR. 2005. Experimental deformation of partially melted granite revisited: implications for the metamorphic crust. *J. Metamorph. Geol.* 23:19–28

Rubin AM. 1993. Dikes vs. diapirs in viscoelastic rock. *Earth Planet. Sci. Lett.* 119:641–59

Rubin AM. 1998. Dike ascent in partially molten rock. *J. Geophys. Res.* 103:20901–19

Rudnicki JW, Rice JR. 1975. Conditions for the localization of deformation in pressure-sensitive dilatant materials. *J. Mech. Phys. Solids* 23:371–94

Rybacki E, Wirth R, Dresen G. 2008. High-strain creep of feldspar rocks: implications for cavitation and ductile failure in the lower crust. *Geophys. Res. Lett.* 35:L04304

Rychert CA, Rondenay S, Fischer KM. 2007. P-to-S and S-to-P imaging of a sharp lithosphere-asthenosphere boundary beneath eastern North America. *J. Geophys. Res.* 112:B08314

Schmocker M, Bystricky M, Kunze K, Burlini L, Stünitz H, Burg J-P. 2003. Granular flow and Riedel band formation in water-rich quartz aggregates experimentally deformed in torsion. *J. Geophys. Res.* 108:2242

Scott DR, Stevenson DJ. 1984. Magma solitons. *Geophys. Res. Lett.* 11:1161–64

Scott DR, Stevenson DJ, Whitehead JA Jr. 1986. Observations of solitary waves in a viscously deformable pipe. *Nature* 319:759–61

Scott T, Kohlstedt DL. 2006. The effect of large melt fraction on the deformation behavior of peridotite. *Earth Planet. Sci. Lett.* 246:177–87

Sleep NH. 1988. Tapping of melt by veins and dykes. *J. Geophys. Res.* 93:10255–72

Spence DA, Sharp P, Turcotte DL. 1987. Buoyancy-driven crack propagation: a mechanism for magma migration. *J. Fluid Mech.* 174:135–53

Spence DA, Turcotte DL. 1985. Magma-driven propagation of cracks. *J. Geophys. Res.* 90:575–80

Spiegelman M. 1993. Flow in deformable porous media. Part 2. Numerical analysis. The relationship between shock waves and solitary waves. *J. Fluid Mech.* 247:39–63

Spiegelman M. 2003. Linear analysis of melt band formation by simple shear. *Geochem. Geophys. Geosyst.* 4:8615

Spiegelman M, Kenyon P. 1992. The requirements for chemical disequilibrium during magma migration. *Earth Planet. Sci. Lett.* 109:611–20

Spiegelman M, McKenzie D. 1987. Simple 2D models for melt extraction at mid-ocean ridges and island arcs. *Earth Planet. Sci. Lett.* 83:137–52

Stevenson DJ. 1986. On the role of surface tension in the migration of melts and fluids. *Geophys. Res. Lett.* 13:1149–52

Stevenson DJ. 1989. Spontaneous small-scale melt segregation in partial melts undergoing deformation. *Geophys. Res. Lett.* 16:1067–70

Takei Y. 1998. Constitutive mechanical relations of solid-liquid composites in terms of grain-boundary contiguity. *J. Geophys. Res.* 103:18183–203

Takei Y. 2000. Acoustic properties of partially molten media studied on a simple binary system with a controllable dihedral angle. *J. Geophys. Res.* 105:16665–82

Takei Y. 2001. Stress-induce anisotropy in partially molten media inferred from experimental deformation of a simple binary system under acoustic monitoring. *J. Geophys. Res.* 106:567–88

Takei Y. 2005. Deformation-induced grain boundary wetting and its effects on the acoustic and rheological properties of partially molten rock analogue. *J. Geophys. Res.* 110:B12203

Takei Y, Holtzman BK. 2007a. Viscous and elastic anisotropy in partially molten rocks. I: Experimental, field, and seismic observations. *Eos Trans. AGU* 88(52) Fall Meet. Suppl., Abstr. T12B-04

Takei Y, Holtzman BK. 2007b. Viscous and elastic anisotropy in partially molten rocks. II: Significant role of viscous anisotropy in melt migration dynamics. *Eos Trans. AGU* 88(52) Fall Meet. Suppl., Abstr. T12B-05

Takei Y, Holtzman B. 2009a. Viscous constitutive relations of solid-liquid composites in terms of grain boundary contiguity I: grain boundary diffusion-control model. *J. Geophys. Res.* In press

Takei Y, Holtzman B. 2009b. Viscous constitutive relations of solid-liquid composites in terms of grain boundary contiguity II: compositional model for small melt fractions. *J. Geophys. Res.* In press

Takei Y, Holtzman B. 2009c. Viscous constitutive relations of solid-liquid composites in terms of grain boundary contiguity III: causes and consequences of viscous anisotropy. *J. Geophys. Res.* In press

Tommasi A, Tikoff B, Vauchez A. 1999. Upper mantle tectonics: three-dimensional deformation, olivine crystallographic fabrics and seismic properties. *Earth Planet. Sci. Lett.* 168:173–86

Vaughan PJ, Kohlstedt DL, Waff HS. 1982. Distribution of the glass phase in hot-pressed, olivine-basalt aggregates: an electron microscopy study. *Contrib. Mineral. Petrol.* 81:253–61

von Bargen N, Waff HS. 1986. Permeabilities, interfacial areas and curvatures of partially molten systems: results of numerical computations of equilibrium microstructures. *J. Geophys. Res.* 91:9261–76

Waff HS, Bulau JR. 1979. Equilibrium fluid distribution in an ultramafic partial melts under hydrostatic stress condition. *J. Geophys. Res.* 84:6109–14

Waff HS, Bulau JS. 1982. Experimental determination of near equilibrium textures in partially molten silicates at high pressure. In *High-Pressure Research in Geophysics*, *Advances in Earth and Planetary Sciences*, ed. S Akimota, MH Manghnani, 12:229–36. Tokyo: Cent. Acad. Publ. 632 pp.

Waff HS, Faul UH. 1992. Effects of crystalline anisotropy on fluid distribution in ultramafic partial melts. *J. Geophys. Res.* 97:9003–14

Walte NP, Bons PD, Passchier CW. 2005. Deformation of melt-bearing systems. Insight from in situ grain-scale analogue experiments. *J. Struct. Geol.* 27:1666–79

Watson BE. 1982. Melt infiltration and magma evolution. *J. Geol.* 10:236–40

Weertman J. 1971. Theory of water-filled crevasses in glaciers applied to vertical magma transport beneath oceanic ridges. *J. Geophys. Res.* 76:1171–83

Whitehead JA. 1987. A laboratory demonstration of solitons using a vertical watery conduit in syrup. *Am. J. Phys.* 55:998–1003

Xu Y, Zimmerman ME, Kohlstedt DL. 2004. Deformation behavior of partially molten mantle rocks. In *Rheology and Deformation of the Lithosphere at Continental Margins: MARGINS Theoretical and Experimental Earth Science Series*, ed. GD Karner, NW Driscoll, B Taylor, DL Kohlstedt, 1:284–310. New York: Columbia Univ. Press

Yoshino T, Takei Y, Wark DA, Watson EB. 2005. Grain boundary wetness of texturally equilibrated rocks, with implications for seismic properties of the upper mantle. *J. Geophys. Res.* 110:B08205

Zhang S, Karato S-I. 1995. Lattice preferred orientation of olivine deformed in simple shear. *Nature* 375:774–77

Zhang S, Karato S-I, Fitz Gerald J, Faul UH, Zhou Y. 2000. Simple shear deformation of olivine aggregates. *Tectonophysics* 316:133–52

Zimmerman ME, Kohlstedt DL. 1996. Rheology of partially molten rocks. *Annu. Rev. Earth Planet. Sci.* 24:41–62

Zimmerman ME, Kohlstedt DL. 2004. Rheological properties of partially molten lherzolite. *J. Petrol.* 45:275–98

Zimmerman ME, Zhang S, Kohlstedt DL, Karato S. 1999. Melt distribution in mantle rocks deformed in shear. *Geophys. Res. Lett.* 26:1505–8